Published in final edited form as:
Astron Astrophys. ; 616: . doi:10.1051/0004-6361/201732518.

The chemistry of disks around T Tauri and Herbig Ae/Be stars

Marcelino Agúndez[1], **Evelyne Roueff**[2], **Franck Le Petit**[2], and **Jacques Le Bourlot**[2,3]

[1]Instituto de Física Fundamental, CSIC, C/ Serrano 123, E-28006 Madrid, Spain

[2]Sorbonne Université, Observatoire de Paris, Université PSL, CNRS, LERMA, F-92190 Meudon, France

[3]Université Paris-Diderot, Sorbonne Paris-Cité, F-75013 Paris, France

Abstract

Context—Infrared and (sub-)mm observations of disks around T Tauri and Herbig Ae/Be stars point to a chemical differentiation between both types of disks, with a lower detection rate of molecules in disks around hotter stars.

Aims—To investigate the underlying causes of the chemical differentiation indicated by observations we perform a comparative study of the chemistry of T Tauri and Herbig Ae/Be disks. This is one of the first studies to compare chemistry in the outer regions of these two types of disks.

Methods—We developed a model to compute the chemical composition of a generic protoplanetary disk, with particular attention to the photochemistry, and applied it to a T Tauri and a Herbig Ae/Be disk. We compiled cross sections and computed photodissociation and photoionization rates at each location in the disk by solving the FUV radiative transfer in a 1+1D approach using the Meudon PDR code and adopting observed stellar spectra.

Results—The warmer disk temperatures and higher ultraviolet flux of Herbig stars compared to T Tauri stars induce some differences in the disk chemistry. In the hot inner regions, H_2O, and simple organic molecules like C_2H_2, HCN, and CH_4 are predicted to be very abundant in T Tauri disks and even more in Herbig Ae/Be disks, in contrast with infrared observations that find a much lower detection rate of water and simple organics toward disks around hotter stars. In the outer regions, the model indicates that the molecules typically observed in disks, like HCN, CN, C_2H, H_2CO, CS, SO, and HCO^+, do not have drastic abundance differences between T Tauri and Herbig Ae disks. Some species produced under the action of photochemistry, like C_2H and CN, are predicted to have slightly lower abundances around Herbig Ae stars due to a narrowing of the photochemically active layer. Observations indeed suggest that these radicals are somewhat less abundant in Herbig Ae disks, although in any case the inferred abundance differences are small, of a factor of a few at most. A clear chemical differentiation between both types of disks concerns ices. Owing to the warmer temperatures of Herbig Ae disks, one expects snowlines lying farther away from the star and a lower mass of ices compared to T Tauri disks.

marcelino.agundez@csic.es.

Europe PMC Funders Author Manuscripts

Conclusions—The global chemical behavior of T Tauri and Herbig Ae/Be disks is quite similar. The main differences are driven by the warmer temperatures of the latter, which result in a larger reservoir or water and simple organics in the inner regions and a lower mass of ices in the outer disk.

Keywords

astrochemistry; molecular processes; protoplanetary disks; stars: variables: T Tauri, Herbig Ae/Be

1 Introduction

Circumstellar disks around young stars, the so-called protoplanetary disks, are an important link in the evolution from molecular clouds to planetary systems. These disks allow to feed with matter the young star and provide the scenario in which planets form. The study of the physical and chemical conditions of these objects is thus of paramount importance to understand how and from which type of material do planets form. Protoplanetary disks are mainly composed of molecular gas and dust. The last two decades have seen significant progress in the study of their chemical composition thanks to astronomical observations at wavelengths from the millimeter to the ultraviolet domains.

Observations with ground-based mm and sub-mm telescopes such as the 30m antenna of the Institut de Radioastronomie Millimétrique (IRAM), the James Clerk Maxwell Telescope (JCMT), and the APEX 12m telescope, which are sensitive to the outer cool regions of disks, have provided information on the presence of various gaseous molecules such as CO, HCO^+, H_2CO, C_2H, HCN, HNC, CN, CS, and SO (Dutrey et al. 1997; Kastner et al. 1997, 2014; van Zadelhoff et al. 2001; Thi et al. 2004; Fuente et al. 2010; Guilloteau et al. 2013, 2016; Pacheco-Vázquez et al. 2015). Interferometers that operate at (sub-)millimeter wavelengths such as the OVRO millimeter array, the IRAM array at Plateau de Bure (PdBI, now known as NOEMA), and the Submillimeter Array (SMA) have also allowed to perform sensitive observations leading to the detection of new molecules such as N_2H^+ and HC_3N, and to obtain maps of the emission distribution of some molecules with angular resolutions down to a few arcsec (Qi et al. 2003, 2008, 2013a; Dutrey et al. 2007, 2011; Piétu et al. 2007; Schreyer et al. 2008; Henning et al. 2010; Öberg et al. 2010, 2011; Chapillon et al. 2012a,b; Fuente et al. 2012; Graninger et al. 2015; Teague et al. 2015; Pacheco-Vázquez et al. 2016). In recent years, the advent of the Atacama Large Millimeter Array (ALMA) is making possible to characterize the molecular content of protoplanetary disks with an unprecedented sensitivity and angular resolution (down to sub-arcsec scales). For example, thanks to ALMA it has been possible to detect new molecules such as cyclic C_3H_2 (Qi et al. 2013b; Bergin et al. 2016), CH_3CN (Öberg et al. 2015), and CH_3OH (Walsh et al. 2016), and to image the CO snowline in a few disks (Mathews et al. 2013; Qi et al. 2013c, 2015; Schwarz et al. 2016; Zhang et al. 2017). Infrared (IR) observations using space telescopes such as *Spitzer* and ground-based facilities such as the Very Large Telescope (VLT) and the Keck Observatory telescopes have provided a view of the molecular content of the very inner regions of protoplanetary disks, where absorption and emission lines from molecules such as CO, CO_2, H_2O, OH, HCN, C_2H_2, and CH_4 have been routinely observed (Lahuis et al. 2006; Gibb et al. 2007; Salyk et al. 2007, 2008, 2011; Carr & Najita 2008, 2011, 2014;

Europe PMC Funders Author Manuscripts

Pontoppidan et al. 2010a,b; Najita et al. 2010, 2013; Kruger et al. 2011; Doppmann et al. 2011; Fedele et al. 2011; Mandell et al. 2012; Bast et al. 2013; Gibb & Horne 2013; Sargent et al. 2014; Banzatti et al. 2017). The launch of the *Herschel Space Observatory* was also very helpful to investigate the chemical content at far-IR wavelengths, with the detection of molecules such as CH^+ (Thi et al. 2011) and NH_3 (Salinas et al. 2016), and the exhaustive characterization of H_2O and OH from the inner to the outer regions (Hogerheijde et al. 2011; Riviere-Marichalar et al. 2012; Meeus et al. 2012; Fedele et al. 2012, 2013; Podio et al. 2013). Probing the molecular gas in the inner regions of disks through the most abundant molecule, H_2, has also been possible thanks to observations at ultraviolet (UV) wavelengths using the *Hubble Space Telescope* (Ingleby et al. 2009; France et al. 2012).

On the theoretical side, the chemical structure of protoplanetary disks has been also widely studied during the last two decades. Early models focused on the one dimensional radial structure of disks along the midplane (Aikawa et al. 1996, 1997, 1999; Willacy et al. 1998; Aikawa & Herbst 1999a), although it was later on recognized that the chemical composition presents also an important stratification along the vertical direction, with a structure consisting of three main layers: the cold midplane where molecules are mostly condensed as ices on dust grains, a warm upper layer where a rich chemistry takes place, and the uppermost surface layer where photochemistry driven by stellar and interstellar far ultraviolet (FUV) photons regulates the chemical composition (Aikawa & Herbst 1999b, 2001; Willacy & Langer 2000; Aikawa et al. 2002). In recent years there has been an interest in identifying the main processes that affect the abundance and distribution of molecules in protoplanetary disks. An important number of studies have addressed in detail the role of processes such as the interaction with FUV and X-ray radiation (Willacy & Langer 2000; Markwick et al. 2002; Bergin et al. 2003; Ilgner & Nelson 2006a; Agúndez et al. 2008; Aresu et al. 2011; Fogel et al. 2011; Walsh et al. 2010, 2012), the interplay between the thermal and chemical structure (Glassgold et al. 2004; Woitke et al. 2009), turbulent mixing and other transport processes (Ilgner et al. 2004; Semenov et al. 2006; Ilgner & Nelson 2006b; Willacy et al. 2006; Aikawa 2007; Heinzeller et al. 2011; Semenov et al. 2011), and the evolution of dust grains as they grow by coagulation and settle onto the midplane regions (Aikawa & Nomura 2006; Fogel et al. 2011; Akimkin et al. 2013). Some studies have investigated the impact of using different chemical networks (Semenov et al. 2004; Ilgner & Nelson 2006c; Kamp et al. 2017) and the sensitivity to uncertainties in the rate constants of chemical reactions (Vasyunin et al. 2008). Various specific aspects of the chemistry of protoplanetary disks have also been addressed in detail as, for example, deuterium fractionation (Willacy 2007; Willacy & Woods 2009; Thi et al. 2010; Furuya et al. 2013; Yang et al. 2013; Albertsson et al. 2014), the formation and survival of water vapour (Dominik et al. 2005; Glassgold et al. 2009; Bethell & Bergin 2009; Du & Bergin 2014), and the formation of particular species such as benzene (Woods & Willacy 2007) and complex organic molecules (Walsh et al. 2014).

Overall, protoplanetary disks are complex systems where many different processes such as gas phase chemistry, interaction with stellar and interstellar FUV photons, transport processes, adsorption and desorption from dust grains, chemical reactions on grain surfaces, and grain evolution are all together governing the chemical composition (see reviews by

Bergin et al. 2007, Henning & Semenov 2013, Dutrey et al. 2014, and Pontoppidan et al. 2014).

Disks are commonly found around young low-mass (T Tauri) and intermediate-mass (Herbig Ae/Be) stars, which have quite different masses and effective temperatures, and thus may affect differently the disk chemical composition. For example, Herbig Ae/Be stars have a higher ultraviolet flux and disks around them are warmer than around T Tauri stars. Indeed, T Tauri and Herbig Ae disks have been extensively observed from millimeter to IR wavelengths and it has been found that the detection rate of molecules (for example, H_2O, C_2H_2, HCN, CH_4, CO_2, H_2CO, C_2H, and N_2H^+) is strikingly lower toward Herbig Ae disks than toward disks around T Tauri stars (Mandell et al. 2008; Schreyer et al. 2008; Pontoppidan et al. 2010a; Öberg et al. 2010, 2011; Fedele et al. 2011, 2012, 2013; Salyk et al. 2011; Riviere-Marichalar et al. 2012; Meeus et al. 2012; Guilloteau et al. 2016; Banzatti et al. 2017). This fact may indicate that there is a marked chemical differentiation between both types of disks. Most theoretical studies on the chemistry of protoplanetary disks have focused on disks around T Tauri-like stars, and only a few have studied Herbig Ae/Be disks (e.g., Jonkheid et al. 2007). Here we present a comparative study in which we investigate the two dimensional distribution of molecules in disks around T Tauri and Herbig Ae/Be stars. In a recent study, Walsh et al. (2015) have investigated the differences in the chemical composition between disks around stars of different spectral type, focusing on the inner disk regions. In this study, we make a thorough investigation of the main chemical differences and similarities between T Tauri and Herbig Ae/Be disks from the inner to the outer disk regions, which to our knowledge has not been investigated in detail. We are particularly concerned with a detailed treatment of the photochemistry and with the impact of the FUV illumination from these two types of stars on the chemical composition of the disk. To this purpose we have implemented the Meudon PDR code in the disk model to compute photodestruction rates at each location in the disk in a 1 + 1D approach. We adopted FUV stellar spectra coming from observations of representative T Tauri and Herbig Ae/Be stars. In Sec. 2 we present in detail our physical and chemical disk model, with a particular emphasis on the photochemistry (further described in Appendices A and B), in Sec. 3 we present the resulting abundance distributions of important families of molecules for our T Tauri and Herbig Ae/Be disk models and compare them with results from observations, in Sec. 4 we analyse the influence on the chemistry of the stellar spectra and the method used to compute photodestruction rates, and we summarize the main conclusions found in this work in Sec. 5.

2 The disk model

We consider a passively irradiated disk in steady state around a T Tauri or Herbig Ae/Be star. We solve the thermal and chemical structure of the disk using a procedure which can be summarized as follows. We first solve the dust temperature distribution in the disk using the RADMC code (Dullemond & Dominik 2004). We assume that gas and dust are thermally coupled except for the surface layers of the disk where we estimate the gas kinetic temperature following Kamp & Dullemond (2004). We then solve the radiative transfer of interstellar FUV photons along the vertical direction and of stellar FUV photons along the direction from the star using the Meudon PDR code (Le Petit et al. 2006) to get the

Europe PMC Funders Author Manuscripts

photodissociation and photoionization rates of the different species at each disk location. We finally solve the chemical composition at each location in the disk as a function of time including gas phase chemical reactions, processes induced by FUV photons and cosmic rays, and interactions of gas particles with dust grains (adsorption and desorption processes).

2.1 Physical model

We adopt a fiducial model of disk representative of objects commonly found around T Tauri and Herbig Ae/Be stars (see parameters in Table 1). The disk extends between an inner radius R_{in} of 0.5 au and an outer radius R_{out} of 500 au from the star and has a mass M_{disk} of 0.01 $M_\odot$. We consider that the radial distribution of the surface density Σ is given by a power law of the type

$$\Sigma = \Sigma_0 \left(r/r_0\right)^{-\epsilon}, \quad (1)$$

where Σ_0 is the surface density at a reference radius r_0 and the exponent ϵ is chosen to be 1.0 between R_{in} and R_{out}. To avoid the abrupt disappearance of the disk at the inner radius we set ϵ to −12 at $r < R_{in}$, which results in a soft continuation of the disk at the inner regions.

We consider that dust is present in the disk with a uniform abundance and size distribution, i.e., which does not vary with radius nor height over midplane. We adopt a gas-to-dust mass ratio of 100 and consider spherical grains typically present in the interstellar medium, i.e., with the composition being a mixture of 70 % of silicate and 30 % of graphite (with optical properties taken from Draine & Lee 1984, Laor & Draine 1993, and Weingartner & Draine 2001), and the size distribution being given by the power law

$$n(a) \propto a^{-\beta}, \quad (2)$$

where $n(a)$ is the number of grains of radius a, the minimum and maximum grain radius a_{min} and a_{max} are 0.001 and 1 μm, and the exponent β takes a value of 3.5 according to Mathis et al. (1977).

As stellar parameters we adopt typical values of T Tauri and Herbig Ae/Be stars. The T Tauri star is assumed to have a mass M_* of 0.5 $M_\odot$, a radius R_* of 2 $R_\odot$, and an effective temperature T_* of ~4000 K, typical values of T Tauri stars of spectral type M0-K7 in Taurus (Kenyon & Hartmann 1995). In the case of the star of type Herbig Ae/Be we adopt a mass of 2.5 $M_\odot$, a radius of 2.5 $R_\odot$, and an effective temperature of ~10,000 K, typical values of early Ae and late Be stars (e.g., Martin-Zaïdi et al. 2008; Montesinos et al. 2009).

2.1.1 Stellar and interstellar FUV spectra—

The irradiation from the central star is of great importance for the disk because it dominates the heating of gas and dust. The stellar and interstellar spectra at FUV wavelengths are also of prime importance because they control the photochemistry that takes place in the disk surface.

The FUV component of the interstellar radiation field (ISRF) adopted here is given by

$$I_\lambda = \frac{1}{4\pi}\left(\frac{6.3622\times10^{7}}{\lambda^4} - \frac{1.0238\times10^{11}}{\lambda^5} + \frac{4.0813\times10^{13}}{\lambda^6}\right), \quad (3)$$

where λ is the wavelength in Å, I_λ is the specific intensity in units of erg s^{-1} cm^{-2} $Å^{-1}$ sr^{-1}, and the expression has been obtained by fitting to the radiation field given by Draine (1978). The expression in Eq. (3) is similar to that given by Le Petit et al. (2006), except for an erratum in their first term. The ISRF given by Eq. (3) is complemented with another component that accounts for the emission at longer wavelengths (from ~2000 Å to the near IR), for which we adopt the radiation field given by Mathis et al. (1983) in the form of a combination of three diluted black bodies

$$I_\lambda = 1.05\times10^{-14}B_\lambda(7127\mathrm{K}) + 1.28\times10^{-13}B_\lambda(4043\mathrm{K}) + 3.30\times10^{-13}B_\lambda(2930\mathrm{K}), \quad (4)$$

where $B_\lambda(T)$ is the Planck law at temperature T.

Concerning stellar spectra, in the case of the T Tauri star we adopt as a proxy of the stellar spectrum that of TW Hya, which consists of observations with the *Far Ultraviolet Spectroscopic Explorer* (FUSE) in the 900-1150 Å wavelength range (data from program C0670102) and *Hubble* STIS observations in the 1150-3150 Å range (Herczeg et al. 2002; Bergin et al. 2003). The intrinsic stellar brightness is calculated adopting a distance to the star of 51 pc (Mamajek 2005), a stellar radius of 1 $R_\odot$ (Webb et al. 1999), and a negligible interstellar reddening (Bergin et al. 2003). At wavelengths longer than 3150 Å we use a Kurucz model spectrum (Castelli & Kurucz 2004)[1] with an effective temperature of 4000 K, a surface gravity of $10^{1.5}$ cm s^{-2}, and solar metallicity, scaled to match the flux of TW Hya around 3150 Å. The resulting spectrum is similar to that presented by France et al. (2014) in the 1150-1750 Å wavelength range, although their continuum level is about twice below our adopted spectrum. In the case of the star of type Herbig Ae/Be we use as a proxy the FUV spectrum of AB Aurigae, which consists of observations taken with FUSE in the 900-1190 Å wavelength range (data from program P2190301) and with *Hubble* STIS in the 1190-1710 Å range (Roberge et al. 2001; Ayres 2010). The intrinsic brightness of AB Aurigae is calculated adopting a distance to the star of 144 pc, a stellar radius of 2.41 $R_\odot$, and an interstellar extinction of 0.48 mag (Martin-Zaïdi et al. 2008). For the correction due to extinction we use the method and coefficients of Fitzpatrick & Massa (2007). Longwards of 1710 Å we use a Kurucz spectrum (Castelli & Kurucz 2004) with an effective temperature of 9750 K (close to that of AB Aurigae), a surface gravity of $10^{2.0}$ cm s^{-2}, and solar metallicity.

The FUV spectra adopted for the T Tauri and Herbig Ae/Be stars are shown in Fig. 1, where we also compare with spectra corresponding to blackbodies at the temperatures of the T Tauri and Herbig Ae/Be stars, 4000 K and 10,000 K, respectively. It is seen that AB Aurigae outshines by 2-3 orders of magnitude the FUV flux of TW Hya because of the much higher

[1] http://wwwuser.oats.inaf.it/castelli

effective temperature. However, T Tauri stars usually have an important FUV excess and may become very bright in lines such as Lyα (at 1215.67 Å). It is worth noting that TW Hya is brighter than AB Aurigae in the Lyα line and that in TW Hya the fraction of flux emitted in Lyα is about 30 % of the total flux emitted in the 910-2400 Å wavelength range. We also note that while the FUV spectra of AB Aurigae is similar to that of a 10,000 K blackbody, a 4000 K blackbody is a bad approximation for a T Tauri star as it completely misses the FUV excess. As will be discussed in Sec. 4, this has important consequences for the chemistry of the disk.

2.1.2 Dust and gas temperature—Given the input parameters characteristic of the star (M_*, R_*, and stellar spectrum), the radial distribution of surface density in the disk given by Eq. (1), the dust-to-gas mass ratio, and the dust properties, we solve for the two dimensional distribution of the dust temperature in the disk using the RADMC code (Dullemond & Dominik 2004)[2]. RADMC is a two dimensional Monte Carlo code that solves the dust continuum radiative transfer in circumstellar disks and yields the dust temperature as a function of radius r and height z over the midplane. The vertical distribution of the volume density of particles $n(z)$ is assumed to be given by hydrostatic equilibrium as

$$\frac{dn(z)}{n(z)} = -\frac{\mu G M_*}{k T_d(z)} \frac{z}{\left(z^2 + r^2\right)^{3/2}} dz, \quad (5)$$

where μ is the mean mass of particles, G the gravitational constant, k the Boltzmann constant, and $T_d(z)$ is the vertical distribution of dust temperature. We proceed iteratively to find $n(z)$ at each radius r according to Eq. (5) and consistently with the vertical distribution of dust temperature $T_d(z)$ computed at each radius r.

We assume that gas and dust are thermally coupled, i.e., gas and dust temperatures are equal, except for the disk surface. Models dealing with the computation of the gas temperature in protoplanetary disks find that the thermal coupling of gas and dust is a good approximation over most of the disk and that this assumption breaks down at the surface layers of the disk, where the visual extinction A_V in the vertical outward direction becomes lower than ~1 (Kamp & Dullemond 2004; Woitke et al. 2009; Walsh et al. 2010). In these surface layers the gas can be much warmer than dust grains. In order to take this into account we use the following approximation for the gas temperature. We assume that the gas temperature is equal to the dust temperature in those regions where A_V in the vertical outward direction is higher than 1. Following the study by Kamp & Dullemond (2004), we assume that in the uppermost regions of the disk, where $A_V < 0.01$, the gas temperature is equal to the evaporation temperature of a hydrogen atom, calculated as the temperature at which the most probable speed of particles equals the escape velocity from the disk, i.e.,

[2] http://www.mpia-hd.mpg.de/~dullemon/radtrans/radmc

$$T_{\rm evap} = \frac{GM_* m_{\rm H}}{kr}, \quad (6)$$

where $m_{\rm H}$ is the mass of a hydrogen atom. Finally, at regions intermediate between $A_V = 1$ and $A_V = 0.01$ we approximate the gas temperature through a linear interpolation with height. In Fig. 2 we show the two dimensional distributions of the volume density of particles and of the gas and dust temperatures calculated for the disks around the T Tauri and Herbig Ae/Be stars. The flared shape, which is apparent in both disks, is more prominent in the T Tauri disk owing to the lower gravity of the star. The most significant difference between the physical structure of both disks is that the disk around the Herbig Ae/Be star is significantly warmer than the disk around the T Tauri star because of the higher stellar irradiation of the former.

2.2 Chemical model

Once the physical structure of the disk (temperature of gas and dust and volume density of particles) is calculated at steady state, we solve for the temporal evolution of the chemical composition at each location in the disk. Since transport processes are neglected, each location in the disk evolve independently of other disk regions. We solve the chemical composition as a function of time up to 1 Myr, which is of the order of the typical ages of protoplanetary disks, for a grid consisting of 50 radii (logarithmically spaced from $R_{\rm in}$ to $R_{\rm out}$) and 200 heights (generated specifically for each radius to properly sample the different regimes of A_V in the vertical direction). The chemical network includes 252 species (97 neutral species, 133 positive ions plus the negative ion H^- and free electrons, and 20 ice molecules) involving the elements H, He, C, N, O, S, Cl, and F. Atoms of Si, P, Fe, Na, and Mg are also included because their ionized forms are important in controlling the degree of ionization in certain disk regions. We adopt as initial chemical composition that calculated with a pseudo-time-dependent chemical model (where the chemical evolution is solved under fixed physical conditions) of a cold dense cloud with standard parameters (density of H nuclei of 2×10^4 cm^{-3}, temperature of 10 K, visual extinction of 10 mag, and cosmic-ray ionization rate of H_2 of 5×10^{-17} s^{-1}) at a time of 0.1 Myr. The elemental abundances adopted, based in the so-called ”low metal” case (e.g., Graedel et al. 1982; Lee et al. 1998), are listed in Table 3 of Agúndez & Wakelam (2013). The chemical network comprises 5533 processes including gas phase chemical reactions, cosmic-ray induced processes, photodissociations and photoionizations due to stellar and interstellar FUV photons, and exchange processes between the gas and ice mantle phases (adsorption and desorption). At this stage, the model does not include X-ray induced processes and grain-surface reactions, except for the formation of H_2. X rays may be an important source of chemical differentiation between disks around T Tauri and Herbig Ae/Be stars because the former are more important X-ray emitters (see, e.g., Telleschi et al. 2007). Moreover, winds and magnetic fields in actively accreting T Tauri systems may lead to cosmic-ray exclusion so that ionization in the disk can be dominated by X rays rather than cosmic rays (Cleeves et al. 2015). Therefore, it will be interesting to study the impact of X rays on the chemistry of the two types of disks in the future. In any case, previous chemical models of T Tauri disks have

Europe PMC Funders Author Manuscripts

found that the gas-phase chemistry is not greatly affected by X rays. The species whose abundance is most affected are, according to Aresu et al. (2011), the ions present in the disk surface OH^+, H_2O^+, H_3O^+, and N^+, while Walsh et al. (2012) find that N_2H^+ is the most sensitive species to X rays. We however note that the models of Aresu et al. (2011) and Walsh et al. (2012) did not consider cosmic-ray exclusion, unlike the study of Cleeves et al. (2015). Chemical reactions occurring on the surface of dust grains are likely to have an effect on the chemical composition of cool midplane regions, especially regarding complex organic molecules (Walsh et al. 2014), although the distribution of abundant molecules and the main chemical patterns in the disk are probably not very much affected by such processes. We also plan to investigate this particular aspect in the future.

2.2.1 Gas phase chemical reactions—The vast majority of gas phase chemical reactions included can be grouped into two main categories: ion-neutral reactions and neutral-neutral reactions. The subset of ion-neutral reactions has been constructed based on databases originally devoted to the study of the chemistry of cold interstellar clouds, such as the UMIST database for astrochemistry (Woodall et al. 2007; McElroy et al. 2013)[3] and the Ohio State University (OSU) database, formerly maintained by E. Herbst and currently integrated into the Kinetic Database for Astrochemistry (KIDA; Wakelam et al. 2012, 2015)[4]. Rate constants of ion-neutral reactions have been taken from the previous databases and from the literature on chemical kinetics. In particular, a large part of the rate constants has been revised according to the compilation by Anicich (2003)[5]. The chemical kinetics of exothermic ion-neutral reactions is rather simple because in most cases the kinetics is dominated by long range electrostatic forces. In the case of reactions in which the neutral species is non polar the theory indicates that the rate constant is independent of temperature and is given by the Langevin value. If the neutral species has an electric dipole moment the expression found by Su & Chesnavich (1982) can be used to evaluate the rate constant and its dependence with temperature (Maergoiz et al. 2009; see more details in Wakelam et al. 2010). For ion-non polar reactions for which there is no experimental data, the rate constant has been approximated as the Langevin value. In the case of ion-polar reactions, we have used the Su-Chesnavich approach to evaluate the rate constant of reactions not studied experimentally and to obtain the temperature dependence of the rate constant of reactions which have been only characterized at one single temperature, usually around 300 K.

The part of the chemical network involving ions includes also dissociative recombinations of positive ions with electrons and radiative recombinations between cations and electrons. The set of reactions and associated rate constants have been mainly taken from databases such as UMIST (Woodall et al. 2007; McElroy et al. 2013) and KIDA (Wakelam et al. 2012, 2015). Information on the chemical kinetics of dissociative recombinations has largely benefited from experiments carried out with ion storage rings (Florescu-Mitchell & Mitchell 2006; Geppert & Lasson 2008).

[3] http://udfa.ajmarkwick.net
[4] http://kida.obs.u-bordeaux1.fr
[5] http://trs.jpl.nasa.gov/handle/2014/7981

The subset of neutral-neutral reactions has been constructed from chemical kinetics databases, such as the one by NIST (Manion et al. 2013)[6], databases devoted to the study of interstellar chemistry, such as UMIST (Woodall et al. 2007; McElroy et al. 2013) and KIDA (Wakelam et al. 2012, 2015), compilations for application in atmospheric chemistry, such as the evaluations by IUPAC (Atkinson et al. 2004, 2006)[7] and JPL (Sander et al. 2011)[8], and compilations for use in combustion chemistry, such as the IUPAC evaluation by Baulch et al. (2005) and the Leeds methane oxidation mechanism (Hughes et al. 2001) or the mechanism by Konnov (2000). A good number of reaction rate constants have been taken from specific experimental and theoretical studies found in the literature on chemical kinetics. For example, we have included the numerous measurements at low and ultra low temperatures carried out with the CRESU apparatus (Smith et al. 2006). It is important to note that some regions of protoplanetary disks may have temperatures up to some thousands of degrees Kelvin and therefore it is necessary to include reactions that become fast at high temperatures, i.e., reactions which are endothermic and/or have activation barriers. Chemical kinetics data for such reactions are to a large extent based on chemical networks used in previous chemical models of warm gas in protoplanetary nebulae (Cernicharo 2004) and inner regions of protoplanetary disks (Agúndez et al. 2008), whose original sources of data are mainly the combustion chemistry databases listed above. A similar high temperature chemical network has also been used by Harada et al. (2010) to model the chemistry of active galactic nuclei of galaxies. We include also three body reactions and their reverse process (thermal dissociation) with H_2, He, and H acting as third body. Three body reactions become important at densities above ~10^{10} cm^{-3}, values that are reached in the innermost midplane regions of protoplanetary disks, while thermal dissociations become important at high temperatures. We use an expanded version of the set of three body reactions and thermal dissociations compiled by Agúndez & Cernicharo (2006). An important aspect of the neutral-neutral subset of reactions is that for many of the endothermic reactions for which chemical kinetics data are not available the rate constants have been calculated through detailed balance from the rate constant of the reverse exothermic reaction and the thermochemical properties of the species involved. Thermochemical data in the form of NASA polynomial coefficients (McBride et al. 2002) have been obtained from compilations like those by Konnov (2000) and Burcat & Ruscic (2005)[9].

2.2.2 Cosmic-ray induced processes—The processes induced by cosmic rays play also an important role in the chemistry of protoplanetary disks. We include the direct ionization of H_2 and atoms by cosmic-ray impact, together with photoprocesses induced by secondary electrons produced in the direct ionization of H_2, the so-called Prasad-Tarafdar mechanism (Prasad & Tarafdar 1983; Gredel et al. 1989). The rates of these processes are expressed in terms of the cosmic-ray ionization rate of H_2 (ζ), for which we adopt a value of 5×10^{-17} s^{-1} (see Table 1), and are taken from astrochemical databases such as UMIST (Woodall et al. 2007; McElroy et al. 2013) and KIDA (Wakelam et al. 2012, 2015).

[6] http://kinetics.nist.gov
[7] http://iupac.pole-ether.fr/
[8] http://jpldataeval.jpl.nasa.gov/
[9] http://burcat.technion.ac.il/dir

Europe PMC Funders Author Manuscripts

2.2.3 Photoprocesses—Photodissociation and photoionization processes caused by stellar and interstellar FUV photons are a key aspect of the chemistry of protoplanetary disks as they control the chemical composition of the surface layers, from where much of the molecular emission arises. In order to treat in detail these processes we have used the Meudon PDR code (Le Petit et al. 2006; Goicoechea & Le Bourlot 2007; González García et al. 2008)[10], where PDR stands for photodissociation region, to compute the photodissociation and photoionization rates of various important species at each location in the disk. We use the version 1.4 of the Meudon PDR code, with some practical modifications to make it more versatile and integrate it into the protoplanetary disk model. The Meudon PDR code solves the FUV radiative transfer in one dimension for a plane-parallel cloud illuminated on one side by a FUV source. In protoplanetary disks the geometry involves two dimensions (radial and vertical) and there are two different FUV sources, the star illuminating from the central position and the interstellar radiation field illuminating isotropically from outside the disk. We thus adopt a 1+1D approach. On the one hand we solve the radiative transfer of FUV interstellar radiation as it propagates from outside the disk to the midplane along a series of vertical directions located at the different radii of the grid described in Sec. 2.2. On the other hand we solve the radiative transfer of FUV stellar radiation as it travels from the star through the disk along a series of directions given by a grid of 200 angles from the midplane (covering the range from 0° to almost 90°). The Meudon PDR code assumes that stellar photons arrive from a direction perpendicular to the plane-parallel surface of the cloud. In disks, the star may illuminate the disk with small grazing angles, in particular in the inner regions where the flaring shape of the disk is less marked. It is thus likely that when computing the FUV energy density along the different directions from the star, at low penetration depths the Meudon PDR code underestimates the contribution of FUV photons scattered by dust from nearby regions around the disk surface. However, it is not straightforward to properly correct by this geometrical effect without moving to 2D and thus we do not apply any specific correction for it here.

In summary, once the physical structure of the disk is calculated at steady state (using the RADMC code as described in Sec. 2.1) and prior to the computation of the temporal evolution of the chemical composition, we use the Meudon PDR code to evaluate the photodissociation and photoionization rates at each location in the disk by calculating the FUV flux as a function of wavelength due to stellar and interstellar radiation and using the relevant wavelength-dependent cross sections. Our approach to treat photochemistry is thus different from other state-of-the-art chemical models of protoplanetary disks in which the FUV radiative transfer is solved in 2D but only in a few broad spectral bands (e.g., Woitke et al. 2016) and it is in essence more similar to the series of models by Walsh et al. (2012, 2014, 2015).

We have compiled cross sections for 29 molecules and 8 atoms (see Appendix A). The photodissociation rate of H_2 and CO are computed by solving the excitation and the line-by-line radiative transfer taking into account self and mutual shielding effects. In the case of photoprocesses for which cross section data is not available we have approximated the rate

[10] http://ism.obspm.fr

using a parametric expression in which the rate Γ, in units of s^{-1}, is expressed as a function of the visual extinction A_V as

$$\Gamma = \chi\alpha\exp(-\gamma A_V), \quad (7)$$

where χ is the FUV[11] energy density with respect to that of the ISRF of Draine (1978), α is the rate under a given unattenuated radiation field with $\chi = 1$, and the coefficient γ controls the decrease in the rate with increasing visual extinction. The coefficients α and γ are specific of each photoprocess and depend also on the spectral shape of the FUV field. Values of α and γ corresponding to the ISRF have been taken from the databases such as the UMIST database for astrochemistry (Woodall et al. 2007; McElroy et al. 2013) and the OSU and KIDA databases (Wakelam et al. 2012, 2015), as well as from the compilation by van Dishoeck et al. (2006), recently revised by Heays et al. (2017).

In Fig. 3 we show the contribution of the stellar and interstellar radiation fields to the photodissociation rate of various molecules as a function of height over the disk midplane. This is shown at two radial distances from the star (1 au and 100 au) for the T Tauri and Herbig Ae/Be disks. We see that in the uppermost regions of the disk, photoprocesses are clearly dominated by the stellar radiation field. However, as we go deeper into the disk, at some point the contribution of the ISRF becomes more important than the stellar one because of the more marked increase of the visual extinction against stellar light than against interstellar photons. Therefore, depending on the location in the disk, photodestruction can be driven by the ISRF or by the star.

2.2.4 Reactions with vibrationally excited H_2—In the disk surface the gas is strongly illuminated by FUV photons and vibrationally excited states of molecular hydrogen are easily populated through FUV fluorescence. Since the reactivity of H_2 can be quite different when it is in the ground or in excited vibrational states –the internal energy of H_2 can be used to overcome or diminish endothermicities or activation barriers which are present when H_2 is in its ground vibrational state– we have included a few reactions of H_2 with specific rate constants for each vibrational state. Concretely, we have included the reactions of H_2 with C^+ (important in the formation of CH^+), He^+, O, OH, and CN, with the rate constant expressions compiled by Agúndez et al. (2010), and the reaction of H_2 and S^+, which may be important in the synthesis of the ion SH^+, with the rate constant expressions calculated by Zanchet et al. (2013). The populations of the different vibrational states of H_2 are computed at each location in the disk with the Meudon PDR code.

2.2.5 Adsorption processes—The adsorption of gas species onto the surface of dust grains is treated in a rather simple and standard way. The adsorption rate of a gas species *i*, in units of s^{-1}, is given by

[11]The FUV is chosen to cover the wavelength range from the Lyman cutoff at 911.776 Å to the limit of the Habing field at 2400 Å.

$$R_i^{ads} = \alpha_i \nu_i \langle \sigma_d n_d \rangle, \quad (8)$$

where α_i and ν_i are the sticking coefficient and thermal velocity of each gas species i. The sticking coefficient is assumed to be 1 for all species and the thermal velocity is evalued as $\sqrt{3kT_k/m_i}$, where T_k is the gas kinetic temperature and m_i is the mass of each gas species i. The term $\langle \sigma_d n_d \rangle$ is the product of the geometric cross section and the volume density of dust particles averaged over the grain size distribution given by Eq. (2) and is evaluated following the formalism of Le Bourlot et al. (1995). To simplify, we only consider adsorption of a limited number of stable neutral species, among which there are the most typically abundant ice constituents (see Table 2).

2.2.6 Desorption processes—Species which have been adsorbed on dust grains forming ice mantles can return to the gas phase through a variety of desorption mechanisms. In protoplanetary disks, the most important desorption processes are thermal desorption and photodesorption by FUV photons. We also include desorption induced by cosmic rays. Based on the results of experimental work using isotopic markers (Bertin et al. 2012, 2013) and molecular dynamics calculations (Andersson & van Dishoeck 2008), we consider that only molecules from the top two monolayers can desorb efficiently ($N_l = 2$). The term due to desorption can therefore be written in the kinetic rate equations as

$$\frac{dn_i}{dt} = -\frac{dn_i^{ice}}{dt} = \left(R_i^{thd} + R_i^{pd} + R_i^{crd}\right) n_i^{ice,\,\mathrm{desorbable}}, \quad (9)$$

where n_i and n_i^{ice} are the volume densities of species i in the gas and ice phases, respectively, R_i^{thd}, R_i^{pd}, R_i^{crd} are the desorption rates, in units of s^{-1}, of thermal desorption, photodesorption, and desorption induced by cosmic rays, respectively (see below). The quantity $n_i^{ice,\,\mathrm{desorbable}}$ is the volume density of species i in the top desorbable ice layers, which is simply equal to n_i^{ice} when these layers are not fully occupied while it is given by n_i^{ice} multiplied by the factor (n_{top}/n_{tot}^{ice}) otherwise. The volume density of sites in the top desorbable layers n_{top} is given by $n_s 4 \langle \sigma_d n_d \rangle N_l$ (where n_s is the surface density of sites, typically $\sim 1.5 \times 10^{15}$ cm^{-2}; see Hasegawa et al. 1992) and n_{tot}^{ice} is the sum of the volume densities of all ice species, i.e., $\Sigma_i n_i^{ice}$. This implementation of desorption in the kinetic rate equations is similar to that of, e.g., Aikawa et al. (1996) and Woitke et al. (2009); see also Cuppen et al. (2017).

– *Thermal desorption.* This process, which depends on the dust temperature T_d and the binding energy of adsorption of each species E_D, controls to a large extent the distribution of ices in protoplanetary disks and the location of the different snow lines of each molecule. The thermal desorption rate, in units of s^{-1}, of an adsorbed species i is given by

$$R_i^{thd} = \nu_{0,i} \exp\left(-E_{D,i}/T_d\right), \quad (10)$$

where $\nu_{0,i}$ is the characteristic vibration frequency of the adsorbed species i (evaluated as $\sqrt{2n_s k E_{D,i}/(\pi^2 m_i)}$, where the binding energy $E_{D,i}$ is expressed in units of K. Binding energies have been measured in the laboratory by depositing volatile species on different cold substrates and using temperature programmed desorption methods (see Burke & Brown 2010 and references therein). In general, binding energies show little dependence with the chemical or morphological nature of the substrate as long as the ice under study consists of various monolayers (ML). If desorption occurs at submonolayer coverage, desorption energies can be quite different depending on the substrate, e.g., they tend to be higher if employing water ice as substrate than using silicates (Noble et al. 2012a). The translation of these laboratory experiments into a realistic model of thermal desorption in protoplanetary disks is complicated because ices are heterogeneous mixtures, thought to be dominated by water ice but whose composition probably varies between cold and warmer regions. Also, molecules may selectively co-desorb with other trapped species, experience volcano desorption following the crystallization of water ice, or co-desorb with some of the major ice constituents (Collings et al. 2004). Here we have adopted the simple and usual approach in which the thermal desorption of each species is controlled by a specific binding energy. We have collected values of E_D experimentally measured, when possible using a water ice substrate and under a submonolayer regime. For those molecules for which experimental binding energies are not available, we have adopted the values estimated by Garrod & Herbst (2006) for a water ice substrate based on the previous compilation by Hasegawa et al. (1993) and the experimental study of Collings et al. (2004). The binding energies of the ice molecules considered and the corresponding references are given in Table 2.

– *Photodtsorption.* The absorption of FUV photons of stellar or interstellar origin (or generated through the Prasad-Tarafdar mechanism) by icy dust grains can induce the desorption of molecules on the ice surface. In regions where the dust temperature is too cold to allow for thermal desorption, photodesorption can provide an efficient means to bring ice molecules to the gas phase. The photodesorption rate, in units of s^{-1}, of an adsorbed species i is given by

$$R_i^{pd} = Y_i F_{\rm FUV} \frac{\langle \sigma_d n_d \rangle}{4 \langle \sigma_d n_d \rangle n_s N_l}, \quad (11)$$

where Y_i is the yield of molecules desorbed per incident photon, $F_{\rm FUV}$ is the FUV photon flux (in units of photon cm^{-2} s^{-1}), and the expression of R_i^{pd} when inserted in Eq. (9), naturally accounts for the fact that ices are not pure but consist of multiple constituents and that desorption is only effective from the top desorbable layers (see, e.g., Cuppen et al. 2017). FUV photons may have an stellar or interstellar origin (in which case $F_{\rm FUV}$ is evaluated with the Meudon PDR code at each position in the disk) or can be generated

through the Prasad-Tarafdar mechanism, in which case we adopt $F_{\rm FUV} = 2 \times 10^3$ photon cm^{-2} s^{-1} (values between 750 and 10^4 photon cm^{-2} s^{-1} have been reported in the literature; e.g., Hartquist & Williams 1990; Shen et al. 2004). Note that this latter value scales with the cosmic-ray ionization rate. Experiments carried out to study the photodesorption of pure ices or binary ice mixtures (Öberg et al. 2009; Muñoz Caro et al. 2010; Fayolle et al. 2011, 2013; Bertin et al. 2013; Fillion et al. 2014; Martín-Doménech et al. 2015) suggest that the main underlying mechanism, called desorption induced by electronic transition (DIET), involves absorption of FUV photons in the ~ 5 top monolayers and electronic excitation of the absorbing molecules, followed by energy redistribution to neighbouring molecules, which may break their intermolecular bonds and be ejected into the gas phase. The efficiency of photodesorption is thus regulated by the ability of the molecules present in the ice surface and sub-surface to absorb FUV photons through electronic transitions. If these transitions are dissociative the situation becomes more complex because the fragments may desorb directly, recombine in the ice and then desorb, or diffuse through the ice forming new molecules that may also desorb (e.g., Andersson & van Dishoeck 2008). Here we adopt a simple approach in which ice molecules may desorb directly or as fragments upon FUV irradiation, with yields based on experimental data for CO, N_2, O_2, H_2O, and CO_2 (see Table 2). Desorption of fragments has been observed upon irradiation of pure ices of H_2O, CO_2, and CH_3OH (Öberg et al. 2009; Fillion et al. 2014; Martín-Doménech et al. 2015; Bertin et al. 2016; Cruz-Diaz et al. 2016), and it is likely that desorption of dissociation fragments and new species formed in situ in the ice dominates over direct desorption for other polyatomic molecules. However, in the absence of experimental photodesorption yields for molecules other than CO, N_2, O_2, H_2O, CO_2, and CH_3OH we have assumed that direct desorption dominates with assumed values for Y_i. It is interesting to note that photodesorption yields of CO, O_2, N_2, CO_2, and CH_3OH have been measured as a function of wavelength using synchrotron techniques (Fayolle et al. 2011, 2013; Fillion et al. 2014; Bertin et al. 2016), which permits to compute the yield Y_i under different FUV fields (see values for the ISRF and the T Tauri and Herbig Ae/Be stellar radiation fields in Table 2). Note for example that the photodesorption yield of CO_2 is almost one order of magnitude higher under the ISRF than under a Herbig Ae/Be stellar field.

- *Cosmic-ray induced desorption.* This mechanism is driven by the impact of cosmic rays on dust grains. The energy deposited on dust grains upon impact of relativistic heavy nuclei of iron results in a local heating that induces the thermal desorption of the ice molecules present in the heated region. According to Hasegawa et al. (1993), the desorption rate induced by cosmic rays, in units of s^{-1}, of a species i is given by

$$R_i^{crd} = 3.16 \times 10^{-19} R_i^{thd}(70\mathrm{K}), \quad (12)$$

where the numerical factor stands for the fraction of the time spent by grains in the vicinity of a temperature of 70 K, at which much of the desorption is assumed to occur in the formalism of Hasegawa et al. (1993), and is derived adopting the Fe cosmic ray flux estimated by Léger et al. (1985) for the local interstellar medium and dust grains with a radius of 0.1 μm. The term R_i^{thd}(70 K) is the rate of thermal desorption of species i, given by

Eq. (10), evaluated at 70 K. The desorption rate R_i^{crd} scales with the cosmic-ray ionization rate.

2.2.7 Formation of H_2 on grain surfaces—The kinetics of H_2 formation on grain surfaces in interstellar space is usually described as

$$\frac{dn(H_2)}{dt} = R_f n_H n(H), \quad (13)$$

where n_H is the volume density of H nuclei, n(H) and $n(H_2)$ are the volume densities of neutral H atoms and H_2 molecules, and R_f is the formation rate parameter for which usually the canonical value of 3×10^{-17} cm^3 s^{-1} derived by Jura (1975) for diffuse interstellar clouds is adopted. Here, we evaluate R_f as

$$R_f = \frac{1}{2} S_H \epsilon_{H_2} \nu_H \langle \sigma_d n_d \rangle \frac{1}{n_H}, \quad (14)$$

where ν_H is the thermal velocity of H atoms, evaluated as $\sqrt{3kT_k/m_H}$. The sticking coefficient of H atoms S_H depends on the gas kinetic temperature T_k and is evaluated through the expression

$$S_H(T_k) = S_0 \frac{(1 + \beta T_k/T_0)}{(1 + T_k/T_0)^\beta}, \quad (15)$$

where we have adopted $S_0 = 1$, $T_0 = 25$ K, and $\beta = 2.5$, based on the experimental study carried out by Chaabouni et al. (2012) for a silicate surface. The recombination efficiency ϵ_{H_2} in Eq. (14) depends on the dust temperature T_d according to the expression derived by Cazaux & Tielens (2002a,b) and is evaluated with the parameters provided by Cazaux & Tielens (2002a) in their Table 1, with an updated value of 12,200 K for the desorption energy of chemisorbed H, as calculated by Goumans et al. (2009) for an olivine surface. Currently, the kinetics of grain-surface H_2 formation considered in the model accounts for the Langmuir-Hinshelwood mechanism. In the future it will be worth to consider also the Eley-Rideal mechanism, which is expected to increase the H_2 formation efficiency at high gas temperatures (e.g., Le Bourlot et al. 2012; Bron et al. 2014).

3 Results

In this section we present the calculated abundance distributions of various molecules in our fiducial T Tauri and Herbig Ae/Be disk models, and compare them with available constraints from observations, with the stress put on the similarities and differences between both types of disks. We focus on molecules that have been observed in disks at IR or (sub-)mm wavelengths. Detected species in disks have been summarized by Dutrey et al. (2014). In

Table 3 we provide an updated an comprehensive summary of the molecules observed in T Tauri and Herbig Ae/Be disks. We first concentrate on molecules observed through IR observations, which are sensitive to the hot inner disk: H_2O and OH (Sec. 3.1), and simple organics such as C_2H_2, HCN, CH_4, and CO_2 (Sec. 3.2). We then focus on molecules observed at (sub-)mm wavelengths, which trace the outer disk: the radicals C_2H and CN (Sec. 3.3) and other organic molecules with a certain complexity, such as H_2CO (Sec. 3.4), the sulfur-bearing molecules CS and SO (Sec. 3.5), and molecular ions (Sec. 3.6). We finally discuss the abundance distributions of ices, for which most observational constraints consist of determining the location of the CO snowline (Sec. 3.7). Abundances are mostly expressed as column densities because this is the quantity provided by most observational studies. Nonetheless, sometimes we use the term fractional abundance, which hereafter refers to the abundance relative to the total number of H nuclei.

3.1 Water and hydroxyl radical

In the last years, near-IR to sub-mm observations have provided important constraints on the presence of water and its related radical (OH) in protoplanetary disks. At near- and mid-IR wavelengths, the spectra of disks around T Tauri stars show emission of hot H_2O and OH arising from the inner disk (< a few au) atmosphere (Carr et al. 2004; Carr & Najita 2008, 2011, 2014; Salyk et al. 2008, 2011; Pontoppidan et al. 2010a,b; Mandell et al. 2012; Sargent et al. 2014; Banzatti et al. 2017), while in disks around Herbig Ae/Be stars, emission by OH is relatively common but there is a striking lack of H_2O emission (Mandell et al. 2008; Pontoppidan et al. 2010a; Fedele et al. 2011; Salyk et al. 2011; Banzatti et al. 2017). Far-IR observations with *Herschel/PACS* have essentially confirmed that the water detection rate is much higher in T Tauri disks than in disks around Herbig Ae/Be stars (Riviere-Marichalar et al. 2012; Meeus et al. 2012; Fedele et al. 2012, 2013). Therefore, infrared observations suggest that water could be intrinsically less abundant in disks around Herbig Ae/Be stars than around T Tauri stars. Such a trend is however not corroborated by our models.

As can be seen in Fig. 4, in the T Tauri disk model, water is present with fractional abundances of ~10^{-4} in a surface layer at A_V~1 in the inner ~10 au from the star, while in the Herbig Ae/Be disk, the warmer temperatures make the region of high H_2O abundance to extend radially beyond 10 au and vertically down to the midplane. In the inner disk, water becomes very abundant in regions warmer than ~200 K, where the reaction OH + H_2 is activated, and sufficiently shielded from FUV photons, while OH is present in a thin layer on top of H_2O resulting from its photodissociation. In our generic T Tauri disk model, the inner midplane regions are not warm enough to sustain a high water abundance, and thus most H_2O (and all OH) are present in upper layers. We however note that the presence of water vapor in the inner midplane is very sensitive to the temperature and that other T Tauri disk models (e.g., Walsh et al. 2015) find high H_2O abundances in these regions. Therefore, the model predicts that as the stellar luminosity increases and the disk becomes warmer water vapor is more abundant.

The vertical column densities calculated for H_2O and OH in the IR-observable atmosphere[12] of the inner T Tauri disk are 10^{17}-10^{18} cm^{-2} and ~10^{15} cm^{-2}, respectively, which are in the

low range of observed values (see left panel in Fig. 5). The calculated OH/H_2O column density ratio in the inner disk, 10^{-2}-10^{-3}, is between the values derived in AA Tau, DR Tau, and AS 205A (0.1-0.3; Carr & Najita 2008; Salyk et al. 2008) and that found from a study of a much larger sample of T Tauri disks (~10^{-3}; Salyk et al. 2011). Previous chemical models of inner T Tauri disks (Agúndez et al. 2008; Walsh et al. 2015) find H_2O and OH column densities and ratios of the same order of magnitude than the ones calculated by us. In summary, chemical models of T Tauri disks predict the existence of an important reservoir of hot water in the inner regions (formed by warm gas-phase chemistry) and smaller amounts of OH (formed by FUV photodissociation of water), with numbers that are roughly in agreement with those derived from IR observations.

In disks around Herbig Ae/Be stars, OH has been detected in about a dozen of objects with a broad range of column densities (see Table 3). In our Herbig Ae/Be disk model, the calculated vertical column density of OH is ~10^{15} cm^{-2} across the first 10 au, decreasing down to ~10^{13} cm^{-2} in the outer disk, in the low range of values derived from observations (see right panel in Fig. 5). Walsh et al. (2015) calculate somewhat higher values for the inner 10 au, 10^{16}-10^{17} cm^{-2}, more in line with the high range of observed values. Water has been convincingly detected at IR wavelengths only around one Herbig star, HD 163296 (Meeus et al. 2012; Fedele et al. 2012). The H_2O and OH column densities derived in this disk are similar, in the range 10^{14}-10^{15} cm^{-2}, and the emitting region for both species is constrained to be 15-20 au from the star. In our Herbig Ae/Be disk model, the column density of water is very large in the inner disk (out to ~4 au), where it is very abundant in the midplane (see right panels in Figs. 4 and 5), and experiences a sharp abundance decline with increasing radius. At 15-20 au from the star, where water is no longer present in the midplane but in upper disk layers, the model yields $N(H_2O)$ = 10^{15}-10^{16} cm^{-2} and $N(OH)$ = 10^{14}-10^{15} cm^{-2}, with a OH/H_2O ratio of ~0.1, values which are not far from those derived in the HD 163296 disk. In the Herbig Ae disk model of Walsh et al. (2015), at 10 au (the farthest radius studied by these authors) the column densities of H_2O and OH are in the range 10^{16}-10^{17}, with the OH/H_2O ratio approaching unity. The model of Walsh et al. (2015) and ours do a reasonable job at explaining the order of magnitude of the water and OH observations of HD 163296. It however remains puzzling to explain the extremely low detection rate of water in Herbig Ae/Be disks, as compared with T Tauri disks, taking into account that chemical models (Walsh et al. 2015 and this work) predict that in disks around Herbig stars, water should be even more abundant than in T Tauri disks. Several explanations have been proposed (see Antonellini et al. 2016 and references therein), most of which are related to observational aspects (e.g., the higher level of infrared continuum in Herbig Ae/Be disks and the lower sensitivity reached for detection of emission lines above the continuum) than with substantive differences in the chemistry between disks around low- and intermediate-mass pre-main sequence stars.

Our model predicts that the reservoir of hot water present in the inner regions of disks around T Tauri and Herbig Ae/Be stars vanishes typically beyond 10 au from the star, owing to thermal deactivation of the water-forming reaction OH + H_2 and to freeze-out onto dust

[12]We consider the IR-observable atmosphere to extend down to the A_V = 10 layer, where the optical depth at 10 μm is of the order of unity.

grains. This drastic decline of various orders of magnitude in the abundance and column density of water (see Figs. 4 and 5) has been observationally probed by mid- to far-IR observations in a few protoplanetary disks (Blevins et al. 2016). The model however predicts that there exists an additional reservoir of cold water in the outer parts of T Tauri and Herbig Ae/Be disks, typically beyond 100 au and at intermediate heights (see Fig. 4). Water in these regions arises from the FUV photodesorption of water ice and reaches peak fractional abundances of ~10^{-7}, with typical vertical column densities of the order of 10^{13}-10^{14} cm^{-2} (see Fig. 5). This outer reservoir of water is also predicted by previous chemical models of T Tauri disks which include photodesorption (e.g., Willacy & Langer 2000; Woitke et al. 2009; Semenov et al. 2011; Walsh et al. 2012) and has been detected with *Herschel/HIFI* in the T Tauri disks TW Hya and DG Tau (Hogerheijde et al. 2011; Podio et al. 2013) and in the Herbig Be disk HD 100546 (van Dishoeck et al. 2014; Du et al. 2017), although it remains elusive to detection in many other protoplanetary disks (Bergin et al. 2010; Du et al. 2017). It is remarkable that the detection rate of water at sub-mm wavelengths is not so different between T Tauri and Herbig Ae/Be disks as it is at IR wavelengths (see Table 3), which suggests that the low detection rate of H_2O IR emission in Herbig objects may not be due to an intrinsic deficit of water with respect to T Tauri systems.

3.2 Simple organics: C_2H_2, HCN, CH_4, and CO_2

It is known that there exists an important reservoir of simple organic molecules in protoplanetary disks. Thanks to observations at near- and mid-IR wavelengths, lines of molecules such as acetylene, hydrogen cyanide, methane, and carbon dioxide have been detected in absorption (Lahuis et al. 2006; Gibb et al. 2007; Gibb & Horne 2013; Bast et al. 2013) and in emission (Carr & Najita 2008, 2011; Salyk et al. 2011; Kruger et al. 2011; Mandell et al. 2012; Najita et al. 2013; Pascucci et al. 2013). These observations probe hot gas located in the inner (a few au) disk, where these molecules are found with large abundances. It is noteworthy that the vast majority of infrared detections of simple organics correspond to disks around T Tauri stars rather than to disks around Herbig Ae/Be stars, where neither C_2H_2, HCN, nor CH_4 are detected, and only CO_2 has been detected in one disk, HD 101412 (Salyk et al. 2011). It is therefore tempting to think that Herbig Ae/Be disks are less rich in simple organics than disks around T Tauri stars. However, similarly to the case of H_2O, we do not find such a trend in our models.

In our T Tauri disk model, C_2H_2, HCN, and CH_4 are formed with high fractional abundances (a few × 10^{-5}) in the atmosphere (A_V~1) of the inner (within a few au) regions of the disk (see Fig. 6). Their synthesis is driven by FUV photochemistry in a warm gas (see Agúndez et al. 2008; Bast et al. 2013; Walsh et al. 2015). In the Herbig Ae/Be disk model, the region over which these molecules have large fractional abundances extends to larger radii compared to the T Tauri disk, as a consequence of the higher temperatures. Moreover, in the Herbig Ae/Be disk, C_2H_2, HCN, and CH_4 are formed abundantly in the inner midplane, where the synthesis is not related to photochemistry but to the fact that the chemical composition tends toward thermochemical equilibrium in these hot, dense, and FUV-shielded regions. Both the T Tauri and Herbig Ae/Be disk models show a progressive disappearance of simple organics as one moves radially from the star, in this order: CH_4, C_2H_2, and HCN. This behavior, already predicted by Agúndez et al. (2008), is a

consequence of the requirements of temperature that each molecule has to activate its corresponding formation routes, with CH_4 being the most demanding. Such a trend is also found in the disk models of Walsh et al. (2015) for C_2H_2 and HCN. Note that CH_4, unlike C_2H_2 and HCN, is also predicted to be moderately abundant in cool midplane regions, where the synthesis is driven by ion-molecule routes. In these regions however the calculated abundance of CH_4 could be especially uncertain if grain-surface chemistry (not included in our models) plays an important role.

The calculated vertical column densities of C_2H_2 and HCN in the IR-observable atmosphere of the inner T Tauri disk (within 1 au from the star) are large, with maxima in the range 10^{15}-10^{17} cm^{-2}, in good agreement with observed values (see left panel in Fig. 5). Observations of T Tauri disks indicate that C_2H_2 and HCN have similar abundances, although there is a significant dispersion, and that they are somewhat less abundant than water vapor (C_2H_2/HCN = 0.04-20; HCN/H_2O = 10^{-3}-10^{-1};Lahuis et al. 2006; Gibb et al. 2007; Carr & Najita 2011; Salyk et al. 2011; Mandell et al. 2012; Bast et al. 2013). These observed ratios are in line with the values found in the T Tauri disk model. Methane has only been detected in one T Tauri disk, GV Tau, in absorption (Gibb & Horne 2013). These authors derive a column density of 2.8×10^{17} cm^{-2} and a rotational temperature of 750 K, which implies that the detected CH_4 is distributed in the inner disk. In GV Tau, CH_4 is somewhat more abundant than C_2H_2 and HCN. Note however that in DR Tau, the non detection of CH_4 in emission implies that it has an abundance similar to or smaller than C_2H_2 and HCN (Mandell et al. 2012). In our T Tauri disk model, CH_4 reaches a column density of the order of those of C_2H_2 and HCN in the IR-observable atmosphere of the inner disk (see left panel in Fig. 5). Neither C_2H_2, HCN, or CH_4 have been observed in Herbig Ae/Be disks, although our model predicts that they should be even more abundant than in T Tauri disks (see Figs. 5 and 6). Similar conclusions are found in the models by Walsh et al. (2015). The lack of simple organics in the spectra of Herbig Ae/Be disks has not been investigated to the extent of the lack of water, but it is likely that observational rather than chemical effects are at the origin of it.

Carbon dioxide has been extensively observed in T Tauri disks but only in one Herbig Ae/Be disk, where the derived column density is within the range of values found in T Tauri disks. In our models, CO_2 is formed abundantly, mostly in the inner disk (< 10 au in the T Tauri disk and < 100 au in the Herbig disk) and over most of the vertical structure (see Fig. 6). The formation of CO_2 occurs in the gas-phase, mainly through the reaction OH + CO, and is less demanding in terms of temperature than the formation of C_2H_2, HCN, and CH_4. Therefore, CO_2 extends over larger radii than the other simple organics. The calculated column density of CO_2 in the IR-observable atmosphere of the inner (< 10 au) T Tauri disk is in the range 10^{16}-10^{18} cm^{-2} (see left panel in Fig. 5), in the high range of observed values. As with the other simple organics, according to the model there is no apparent chemical reason for a lower amount of CO_2 in disks around Herbig Ae/Be stars than in T Tauri disks.

The simple organic molecules discussed here experience a drastic decline in their column densities with increasing radius, especially for C_2H_2 and HCN (see Fig. 5). This extended and cooler reservoir of simple organics can be probed at mm wavelengths in the case of polar molecules like HCN. In fact, HCN has been extensively characterized this way in

protoplanetary disks (Dutrey et al. 1997; Thi et al. 2004; Fuente et al. 2010, 2012; Öberg et al. 2010, 2011; Chapillon et al. 2012a; Kastner et al. 2014; Guilloteau et al. 2016). Although the statistics of Herbig Ae disks is low, these studies suggest that T Tauri disks can retain in their outer parts somewhat larger HCN abundances than Herbig Ae disks (see Table 3). The column densities calculated for HCN beyond 100 au are ~10^{13} cm^{-2} in both the T Tauri and the Herbig Ae/Be disks, in the high range of observed values (see Fig. 5). The model predicts a slightly higher amount of HCN in the outer regions of the T Tauri disk compared to the Herbig disk. It is interesting to note that the contrary is found in the inner regions. The reason is that the chemical synthesis of HCN is different in nature in the hot inner disk than in the cool outer regions. In the outer disk (>100 au), HCN is mainly present at intermediate heights with fractional abundances of ~10^{-8} relative to H_2 (see Fig. 6). In these regions, HCN is formed by the same gas-phase chemical routes that operate in cold interstellar clouds, i.e., through ion-molecule reactions that lead to the precursor ion $HCNH^+$, which by dissociative recombination yields HCN as well as its isomer HNC. Thus, both observations and our model suggest that HCN is somewhat more abundant in the outer regions of T Tauri disks compared to Herbig Ae/Be disks. We however caution that on the observational side, the statistics of Herbig Ae disks is low, and on the theoretical one, the difference is small and could result from the particular set of parameters adopted in the models.

Hydrogen isocyanide, closely related to HCN from a chemical point of view, has been only detected around the T Tauri stars DM Tau and TW Hya and the Herbig Ae star HD 163296 (Dutrey et al. 1997; Graninger et al. 2015). The lower detection rate of HNC in disks compared to its most stable isomer HCN suggests that HNC is less abundant than HCN, although there is also a selection effect as lines of HNC have not been targeted as often as those of HCN (e.g., Öberg et al. 2011; Guilloteau et al. 2016). Observations indicate that HNC is indeed somewhat less abundant than HCN, with HNC/HCN ratios in the range 0.1-0.4 (see Table 3). These values may need to be revised down due to differences in the collisional excitation rate coefficients of HCN and HNC (Sarrasin et al. 2010). The calculated distribution of HNC approximately follows that of HCN, but at a lower level of abundance (see Fig. 5). The model shows that there is a gap in the column density of HNC which occurs at 1-10 au in the T Tauri disk (shifted to larger radii in the Herbig Ae/Be disk). There is observational evidence of such a gap in the distribution of HNC from SMA interferometric observations of TW Hya (Graninger et al. 2015). While the presence of HNC in the hot inner disk is related to the existence of large amounts of HCN, a fraction of which isomerizes to HNC in the hot gas phase, in the cool outer disk, HNC has an abundance of the order of that of HCN because the two isomers share the same chemical formation routes, with the molecular ion $HCNH^+$ as main precursor. The calculated HNC/HCN ratio in the outer disk (>100 au) is 0.3-0.4 in both the T Tauri and the Herbig Ae/Be disks, in line with the values derived from observations. Interferometric observations indicate that HNC does not extend out to radii as large as HCN in TW Hya (Graninger et al. 2015), a feature that is not predicted by our T Tauri disk model. A possible explanation could be related to an enhanced photodissociation cross section of HNC compared to that of HCN, something that is suggested by theoretical calculations (Chenel et al. 2016; Aguado et al. 2017).

3.3 Radicals C_2H and CN

The radicals C_2H and CN, usually considered as good tracers of regions affected by FUV radiation such as PDRs, are among the most conspicuous molecules detected in protoplanetary disks at mm wavelengths. These observations probe the emission from the outer disk, out to some hundreds of au from the star. Constraints on the abundances of C_2H and CN mainly come from observations of a few protoplanetary disks, the widely studied T Tauri disks DM Tau, LkCa 15, and TW Hya, and the Herbig Ae disks HD 163296, MWC 480, and AB Aur (Thi et al. 2004; Schreyer et al. 2008; Henning et al. 2010; Fuente et al. 2010; Chapillon et al. 2012a; Kastner et al. 2014) and from the more recent study of Guilloteau et al. (2016), in which a larger sample of disks was observed. These studies suggest that C_2H and CN can reach higher abundances in T Tauri disks than in Herbig Ae disks (see Table 3). This would be in line with the general observational finding of a higher detection rate of molecules in T Tauri disks compared to Herbig Ae disks (e.g., Öberg et al. 2011; Guilloteau et al. 2016). However, the confirmation of such hypothesis is still hampered by the low statistics of Herbig Ae disks observed to date. Observations indicate that C_2H is present with an abundance similar to that of CN in most disks, with C_2H/CN ratios in the range 0.2-3.5 (Guilloteau et al. 2016), and no significant difference between T Tauri and Herbig Ae disks. It is also found that the CN radical is significantly more abundant than HCN in all observed disks, with CN/HCN abundance ratios in the range 4-30 (Guilloteau et al. 2016), and again no substantive difference between T Tauri and Herbig Ae disks. In summary, observations at mm wavelengths tell us that T Tauri disks can retain in the outer regions larger abundances of C_2H and CN than Herbig Ae disks, and that in round numbers the C_2H/CN ratio is ~ 1 and the CN/HCN ratio is ~ 10 in both types of disks. It is also interesting to note that recent ALMA observations have found that C_2H emission shows a ring-like distribution in the TW Hya and DM Tau disks (Bergin et al. 2016).

In the T Tauri and Herbig Ae/Be disk models, C_2H and CN are essentially located in a relatively thin layer in the disk surface, between the $A_V = 1$ and $A_V = 0.01$ layers (see Fig. 7), with vertical column densities of the order of 10^{13} cm^{-2} in the outer disk (see Fig. 8). Protoplanetary disks can be seen as a PDR with the typical layered structure CO/C/C$^+$ along the vertical direction, and C_2H and CN become abundant in the layer where neutral atomic carbon reaches its maximum abundance. The formation of C_2H and CN is therefore associated to the disk PDR and to the availability of atomic C in a FUV illuminated gas. Our results regarding the T Tauri disk are similar to those of previous models of disks around low-mass young stars (e.g., Aikawa & Herbst 1999b, 2002; Willacy & Langer 2000; van Zadelhoff et al. 2003; Willacy et al. 2006; Walsh et al. 2010; Semenov et al. 2011). There are some differences between the T Tauri and the Herbig Ae/Be disks. The higher gravity of the Herbig Ae/Be star makes the layer containing C_2H and CN to be more compressed toward lower heights (see Fig. 7), although the most significant difference is that the calculated column densities of C_2H and CN in the outer disk are somewhat lower in the Herbig Ae/Be disk (see Fig. 8). The reason is that the Herbig disk is illuminated by a more intense FUV field from the star than the T Tauri disk, and this narrows the photochemically active layer and limits the ability of photochemistry to build molecules, resulting in smaller amounts of molecules specifically formed by the action of photochemistry. This is a general difference between disks around T Tauri and Herbig stars that is better appreciated in the

cool outer disk (>100 au), where warm gas-phase chemistry is inhibited and thus cannot counterbalance the effect of FUV photons. For example, beyond 100 au, the radical OH (a species typically formed under the action of photochemistry) is significantly more abundant in the T Tauri disk than in the Herbig disk (see Fig. 5). In the case of C_2H and CN, the fact that the abundances are lower in the Herbig disk is linked to a slight defficiency in the abundance of neutral atomic carbon, which is a key starting point to form both C_2H and CN. The calculated column densities of C_2H and CN are in line with the values derived from observations. Moreover, the slight overabundance (a factor of a few) of these radicals in the T Tauri disk compared to the Herbig Ae/Be disk is in line the observational suggestion that T Tauri disks can retain higher abundances of these two radicals. Another salient feature of the model is that the column densities of both C_2H and CN increase with increasing radius in both the T Tauri and the Herbig Ae/Be disks. The predicted inner gap could be consistent with the ring-like distribution found for C_2H in the TW Hya and DM Tau disks (Bergin et al. 2016). These authors however propose an scenario in which the ring morphology observed for C_2H, and also for cyclic C_3H_2, is related to the evolution of ice-coated dust due to the combined effect of coagulation, gravitational settling, and drift.

The model indicates that HCN is much more abundant than CN in the inner regions of both types of disks, although as one moves away from the star, the CN/HCN ratio increases, reaching values above unity at radii >50 au (see Fig. 8). The overabundance of CN with respect to HCN in the outer disk is in agreement with observations. According to the model, in the outer disk C_2H and CN do not spatially coexist with HCN, the radicals being exclusively present in a relatively thin layer at the disk surface while HCN is located at lower heights. There is some controversy regarding the region where C_2H and CN are present in T Tauri disks because mm observations derive low excitation temperatures ($\lesssim$10 K) for these two radicals (Henning et al. 2010; Chapillon et al. 2012a; Hily-Blant et al. 2017), which suggest that the emission could arise from cold midplane regions rather than from the warm disk surface. If true, this would be in strong disagreement with the predictions of our model and previous chemical models of T Tauri disks (e.g., Aikawa & Herbst 1999b, 2002; Willacy & Langer 2000; van Zadelhoff et al. 2003; Willacy et al. 2006; Walsh et al. 2010; Semenov et al. 2011), which also locate the radicals C_2H and CN well above the midplane. Observations and chemical models of T Tauri disks could still be reconciled if in the outer regions (>100 au) of the surface layer containing C_2H and CN (where densities are in the range 10^5-10^6 cm^{-3} and gas kinetic temperatures are between 30 K and 100 K) these two radicals are subthermally excited. Note however that this could have implications for the column densities derived from observations under the assumption of local thermal equilibrium (LTE). Dedicated non-LTE excitation and radiative transfer calculations (e.g., Aikawa et al. 2002) and comparison with mm observations are needed to shed light on this issue.

3.4 Organic molecules of a certain complexity

In this section we briefly comment on various organic molecules observed in disks that are more complex than those treated in Sec. 3.2. We refer to H_2CO and CH_3OH, the hydrogenation descendants of carbon monoxide, the cyanides HC_3N and CH_3CN, and the cyclic isomer of the hydrocarbon C_3H_2.

Formaldehyde has been quite commonly observed in protoplanetary disks, with a higher detection rate in T Tauri disks than in Herbig Ae disks (Öberg et al. 2010, 2011; Guilloteau et al. 2016), but very similar column densities, a few times 10^{12} cm^{-2}, in both types of disks (see Table 3). Interferometric observations of the disks DM Tau, TW Hya, and HD 163296 have provided interesting constraints on the distribution and origin of H_2CO (Qi et al. 2013a; Loomis et al. 2015; Öberg et al. 2017; Carney et al. 2017). These observations point to the presence of an inner component, consistent with gas-phase formation, and an abundance enhancement in the outer disk (beyond the CO snowline) resulting from formation on grain surfaces by hydrogenation of CO ice followed by desorption. The recent detection of methanol in the TW Hya disk (Walsh et al. 2016) also points to a similar outer disk origin driven by the hydrogenation of CO ice. In our model, which does not include grain-surface chemistry, calculated column densities in the outer regions of the T Tauri and Herbig Ae/Be disks are around 10^{12} cm^{-2} for H_2CO (i.e., not far from observed values), but vanishingly small for CH_3OH. We note that if most of the H_2CO and CH_3OH in the outer disk indeed come from CO ice through grain-surface chemistry, one should expect a significant differentiation between T Tauri and Herbig disks because the latter are warmer and should have a lower reservoir of the precursor CO ice.

Other relatively large organic molecules observed in disks are HC_3N, CH_3CN, and cyclic C_3H_2 (see Table 3). Observations indicate that these molecules are present in the outer disk, out to a few hundreds of au. In these regions, our model predict column densities below the observed values by 1-2 orders of magnitude. Calculated column densities for these molecules are quite different among chemical models in the literature. For example, for HC_3N, Chapillon et al. (2012b) calculate column densities 1-2 orders of magnitude above the observed ones, while Walsh et al. (2014) find values ten times lower than observed. The dispersion of calculated column densities between different chemical models and the poor agreement with observations suggests that the chemistry of these moderately complex molecules is not yet as robust as for smaller species.The probable role of grain-surface reactions in regulating their abundances makes it worth to revisit their chemistry in T Tauri and Herbig Ae disks with an expanded chemical network including grain-surface chemistry.

We note that our model predicts that organic molecules like H_2CO, CH_3OH, HC_3N, CH_3CN, and *c*-C_3H_2 are enhanced in the warm inner regions (within a few au from the star), in particular in the Herbig Ae/Be disk, following the abundance enhancement of simple organics such as C_2H_2 and HCN (see Fig. 5). Such inner reservoir of complex organics, which is the result of hot gas-phase chemistry, could be detectable at millimeter wavelengths with ALMA provided the angular resolution and sensitivity are high enough.

3.5 Sulfur-bearing molecules: CS and SO

A couple of sulfur-bearing molecules, CS and SO, have been detected in protoplanetary disks. The observation of these species is interesting because it provides information on the degree of depletion of sulfur and because they can be used to probe phenomena such as turbulence and dust traps (Guilloteau et al. 2012; Pacheco-Vázquez et al. 2016). CS was among the first molecules detected in disks (Dutrey et al. 1997) and since then has been observed in various T Tauri disks and in two Herbig Ae disks, while SO was first observed

in the Herbig Ae disk AB Aur and has later on been observed in a couple of T Tauri disks (see references in Table 3). These observations were carried out at mm wavelengths and thus trace the outer regions of disks. Although the statistics of observed disks is small, it seems that both CS and SO have column densities of the order of 10^{12}-10^{13} cm^{-2} and that there is no substantial difference between T Tauri and Herbig Ae disks (see Table 3).

In our model, both CS and SO are mostly distributed in a layer located at intermediate heights (around $A_V \sim 1$), both in the T Tauri and the Herbig Ae/Be disks (see Fig. 9). In the inner regions (within a few au from the star) of the Herbig Ae/Be disk, these two molecules extend down to lower heights. The main formation pathways to both molecules involve various fast neutral-neutral reactions and thermal desorption from dust grains. The calculated column densities in the outer disk (beyond 100 au) are around 10^{12} cm^{-2} in both the T Tauri and the Herbig Ae/Be disks, in line with the values derived from observations (see Fig. 8). The S-bearing molecule SO_2 has not been detected in disks but it is predicted to have column densities of the same order or slightly lower than SO in the outer disk (see Fig. 8). In the inner regions, the column densities of CS, SO, and SO_2 are enhanced by various orders of magnitude, especially in the case of the Herbig Ae/Be disk, although these regions are likely to be strongly spatially diluted in the mm observations.

The column densities of CS and SO calculated here for the Herbig Ae/Be disk are similar to those obtained in the chemical model of the AB Aur disk presented by Fuente et al. (2010) and Pacheco-Vázquez et al. (2015). The main difference is that those models predict an enhancement in the column densities of CS and SO in the 100-200 au region, something that is not seen in the Herbig Ae/Be disk model presented here. The main reason of such difference is that those models assumed a more simplistic initial composition, with all the sulfur being initially in the form of CS, while in the present model we adopt a more realistic initial composition in which sulfur is initially distributed in various forms, mostly as S, S^+, CS, and CS ice (see Sec. 2.2). The choice of the initial composition can have non-negligible effects on the calculated abundances at ages typical of protoplanetary disks, something that we plan to investigate in detail in the future.

3.6 Molecular ions

The molecular ion HCO^+ is probably one of the most widely observed species in protoplanetary disks (see references in Table 3). In fact, it is remarkable that the detection rate of HCO^+ is 100 % in all the T Tauri and Herbig Ae disks targeted by Öberg et al. (2010, 2011) and by Guilloteau et al. (2016). Observed column densities are of the order of 10^{12} cm^{-3}, with no significant difference between T Tauri and Herbig Ae disks (see Table 3). In our model, HCO^+ is mainly present in the outer disk at intermediate heights (see Fig. 10), where it is mainly formed by the reaction between H_3^+ and CO. The calculated vertical column density in the outer disk is in the range 10^{12}-10^{13} cm^{-2} in both the T Tauri and the Herbig Ae/Be disks, in good agreement with the values derived from observations (see Fig. 11) and in line with results from previous chemical models of T Tauri disks (e.g., Aikawa & Herbst 1999b, 2002; van Zadelhoff et al. 2003; Walsh et al. 2010, 2012; Semenov et al. 2011). Unlike in the Herbig Ae/Be disk model, in the T Tauri disk model the column density of HCO^+ (and other molecular ions) experience a decline beyond ~200 au. In these outer

regions, the upper layers are more exposed to stellar FUV photons due to the flared shape of the disk, and atomic ions are favored at the expense of polyatomic ions such as HCO^+. This effect is probably a consequence of the particular geometry of the disk model adopted here and may not be a general characteristic of T Tauri disks. Therefore, according to the model, there is no reason to expect significantly different HCO^+ column densities in T Tauri and Herbig Ae disks.

Molecular ions other than HCO^+ are difficult to observe in protoplanetary disks. Nevertheless, sensitive observations with (sub-)mm interferometers have enabled the detection of N_2H^+ in a few T Tauri disks and one Herbig Ae disk, HD 163296 (see references in Table 3). Derived column densities are highly dependent on each source and on each particular study. For example, in the disk around LkCa 15, Qi et al. (2003) derive $\mathcal{N}(N_2H^+) = 3.1 \times 10^{13}$ cm^{-2} from observations with the OVRO array, while Dutrey et al. (2007) find a column density around 100 times smaller using IRAM PdBI. The chemistry of N_2H^+ is relatively simple as it is formed by the reaction between H_3^+ and N_2, which is favored in the coldest regions where CO is mostly in the form of ice, that is, in the outer midplane region. In our particular disk models, CO ice is present beyond a few tens of au in the T Tauri disk, while in the Herbig Ae/Be disk, due to the much warmer dust temperatures, it is barely formed just in the outer edge (see Sec. 3.7). As a consequence, N_2H^+ is present in the outer T Tauri disk with a vertical column density of $\sim 10^{11}$ cm^{-2} while it is almost absent in the Herbig Ae/Be disk (see Fig. 11). The vertical column densities calculated for N_2H^+ are in line with the low range of observed values in the case of the T Tauri disk, while in the Herbig Ae/Be disk, $\mathcal{N}(N_2H^+)$ is lower than observed in HD 163296 by more than one order of magnitude (see Fig. 11). The model also predicts that N_2H^+ must have a ring-like distribution with an inner gap, something that has been verified observationally in the TW Hya disk (Qi et al. 2013c). The inner radius and vertical column density calculated for N_2H^+ are highly dependent on which is the dust temperature structure across the disk, which in turn depends on parameters such as the stellar luminosity, the size and optical properties of dust grains, and the disk geometry (flared vs flat). In any case, since disks around Herbig Ae/Be stars are expected to be significantly warmer than around T Tauri stars, one should expect larger amounts of N_2H^+ in T Tauri disks than in Herbig Ae/Be disks.

Some deuterated ions, mostly DCO^+ but also H_2D^+ and N_2D^+, have been observed at (sub-)mm wavelengths in a few protoplanetary disks (van Dishoeck et al. 2003; Ceccarelli et al. 2004; Guilloteau et al. 2006; Qi et al. 2008; Öberg et al. 2010, 2011, Mathews et al. 2013; Huang & Öberg 2015; Teague et al. 2015; Huang et al. 2017). Here we do not specifically model deuterium chemistry (see, e.g., Willacy 2007; Teague et al. 2015), but we point out that these molecular ions are usually present in the cool outer disk and are useful to probe the fractional ionization. Estimates of the ionization fraction from observations of H_2D^+ (which is present in the midplane of the cold outer disk) are a few times 10^{-10} (Ceccarelli et al. 2004), while values inferred from observations of DCO^+ (which is expected in upper layers than H_2D^+) are as high as $\sim 10^{-7}$ (Qi et al. 2008; Teague et al. 2015). In our T Tauri and Herbig Ae/Be disk models, the ionization fraction in the midplane ranges from $\sim 10^{-10}$ in the denser inner regions to $\sim 10^{-8}$ in the outer disk (see Fig. 10). In these midplane regions, the fractional ionization is controlled by the cosmic-ray ionization rate and also

depends on the gas density. As one moves to upper layers, where the gas is less dense, warmer, and less shielded against interstellar and stellar FUV photons, the ionization fraction increases gradually up to very high values in the surface of the disk (see Fig. 10). According to the model, there are no substantive differences in the ionization degree of disks around T Tauri and Herbig Ae/Be stars.

The ion CH^+ has been detected in a couple of disks, around the Herbig Be star HD 100546 and the Herbig Ae star HD 97048, using *Herschel* (Thi et al. 2011; Fedele et al. 2013). The analysis of the emission lines in HD 100546 indicates that CH^+ has an excitation temperature of 100-300 K, with most emission arising from regions inner to 100 au. In our model, CH^+ is distributed along a surface layer on top of HCO^+ (see Fig. 10), where it is mainly formed by the reaction of C^+ with hot H_2 and FUV-pumped vibrationally excited H_2 (Agúndez et al. 2010) and reaches maximum fractional abundances of ~ 10^{-7}. The calculated distribution of CH^+ is very similar in the T Tauri and Herbig Ae/Be disks. The model predicts that the largest column densities are reached in the outer disk (>100 au; see Fig. 11) contrary to what observations of HD 100546 indicate. We however note that CH^+ emission is probably very sensitive to the temperature structure and geometry of each particular disk. In fact, CH^+ has only been detected in a couple of disks from the sample of 22 Herbig Ae/Be and 8 T Tauri systems surveyed by Fedele et al. (2013).

Apart from HCO^+, the most abundant molecular ions in the disk are H_3^+, CH_2^+, CH_3^+ (see Fig. 11), and $C_2H_2^+$, species which are very difficult to detect. While H_3^+ is mostly present in the midplane of the outer disk, the hydrocarbon cations are essentially present in the disk surface. For example, the formation of CH_2^+ and CH_3^+ is strongly linked to that of CH^+ (Agúndez et al. 2010). Molecular ions not yet observed in disks but potentially detectable are $HCNH^+$ (the precursor of HCN and HNC in the outer disk) and CF^+ (formed in the disk PDR). Both ions are polar and have column densities in excess of 10^{11} cm^{-2} (see Fig. 11), although detecting them may be challenging because their dipole moments are not very high. An additional interesting feature emerging from the model is that most of the positive charge is not carried out by molecular ions but by atomic ions (metals in the disk midplane and carbon in the disk surface).

3.7 Ices and snowlines

Ices account for an important percentage of the matter of protoplanetary disks. The high densities and cold temperatures prevailing in the midplane regions ensure a rapid and efficient adsorption of gas-phase molecules onto dust grains, where they settle and live long in the form of ice. The presence or absence of a particular type of ice in a certain disk region depends on the balance between adsorption and desorption, and, because adsorption rates are similar for most molecules (see Sec. 2.2.5), the extent of each particular type of ice is determined by its specific desorption rate. According to the model, among the various desorption mechanisms considered (see Sec. 2.2.6), thermal desorption is clearly the most important and the one that shapes the bulk distribution of most ices. We however note that for those species with large binding energies, the vertical extent of ices in the outer disk is essentially controlled by photodesorption by interstellar and stellar FUV radiation. In these

outer regions, dust temperatures may not be high enough to trigger thermal desorption of strongly bonded ices, while FUV photons can penetrate down to intermediate heights and provide an efficient means of desorbing ice molecules. The main effect of photodesorption is that it shifts down the snowline[13] of highly polar molecules in the outer disk, enhancing their gas-phase abundance at intermediate heights. In summary, the distribution of ices with low binding energies, such as CO and N_2, is controlled by thermal desorption while for ices with large binding energies, like NH_3 and H_2O (see Table 2), their distribution is determined by thermal desorption in the inner regions and by photodesorption in the outer disk. Other desorption mechanisms, such as cosmic-ray induced desorption or photodesorption by FUV photons generated through the Prasad-Tarafdar mechanism, are much less important.

In protoplanetary disks, ices are mostly distributed around the midplane, from the very outer disk down to an inner edge, which is given by the location of the snowline in the midplane. Since the midplane snowline is essentially controlled by thermal desorption (and thus by the binding energy of the particular ice and by the dust temperature structure of the disk along the midplane), ices appear progressively in the radial direction according to their binding energies. In Fig. 12, we show the calculated distributions of CO and H_2O ices in the T Tauri and Herbig Ae/Be disks. First focusing on the T Tauri disk model, we see that CO ice, for which the adopted binding energy is 1575 K, is only present beyond a few tens of au, while H_2O ice, which has a much higher binding energy (the adopted value is 5773 K), is present all over the disk midplane. The fact that water ice extends down to the inner disk edge is a particular outcome of the T Tauri disk model adopted here, which results in dust that is too cold to allow for efficient thermal desorption of water ice in the inner disk midplane. Since dust temperatures are strongly dependent on parameters such as the size of dust grains, other T Tauri disk models may find outer water snowlines compared to that obtained here (see, e.g., Walsh et al. 2015). An obvious difference between the T Tauri and the Herbig Ae/Be disk models is that in the later, snowlines shift to larger radii owing to the warmer dust temperatures (see Fig. 12) and as a consequence the mass of ices in the disk becomes smaller.

The abundance distributions of CO and H_2O ices shown in Fig. 12 serve to illustrate two extreme cases of molecules with low and high, respectively, binding energies (see Table 2). Other ices with binding energies between those of CO and H_2O have intermediate distributions between those of these two molecules. In general, the smaller the binding energy, the snowline shifts to larger radii. This relationship is illustrated in Fig. 13, where we plot the radius at which the midplane snowline lies for various ices as a function of their binding energies. There is a clear trend which indicates that both quantities are related by a power law of the type $E_D \propto r_{ms}^{-q}$, where $r_{\rm ms}$ stands for radius of midplane snowline. A fit to the data points in Fig. 13 yields an exponent q of ~0.23 in both the T Tauri and the Herbig Ae/Be disks. This behavior is not surprising since the midplane snowline of a given ice is essentially located at the radius at which the dust temperature in the midplane becomes similar to the condensation temperature of the ice, and the latter is directly proportional to the binding energy of the ice. That is, the observed relation between binding energy and

[13]The snowline of a particular species is defined here as the transition region where its gas and ice abundances become equal.

midplane snowline merely reflects how the midplane dust temperature varies with radius. In Fig. 13 we have overplotted as a solid line the radial profile of the dust temperature in the midplane scaled up by a factor of 45. The comparison between solid line and data points in Fig. 13 suggests that a factor of proportionality between binding energy and condensation temperature in the range 30-50 is adequate for the protoplanetary disks modeled here. For comparison, Hollenbach et al. (2009) calculate this factor of proportionality to be ~50 while Martín-Doménech et al. (2014) quote a value of ~30 (from Attard & Barnes 1998).

Using observations to reveal the location of snowlines in protoplanetary disks is still challenging, although ALMA observations are starting to put interesting constraints. For example, in the disk around the T Tauri star TW Hya the CO snowline has been found to lie at a radius of ~ 20 au (Schwarz et al. 2016; Zhang et al. 2017), while in the disk around the Herbig Ae star HD 163296 it has been located at a radius of 90 au from the star (Qi et al. 2015). These two observational points are included in Fig. 13. While the CO snowline derived for TW Hya is close to the value calculated in our T Tauri disk model, the radius derived for HD 163296 is much farther in than indicated by our Herbig Ae/Be disk model, which puts the CO snowline even beyond the outer disk edge. We however note that the coincidence in the case of TW Hya is very likely accidental because our generic T Tauri disk model is not aimed to represent neither the TW Hya disk nor any other particular disk. The observational finding of an outer CO snowline in the HD 163296 disk than in the TW Hya disk is in line with the general expectation that snowlines are shifted to larger radii in Herbig Ae/Be disks compared to T Tauri disks, although it may be also fortuitous taking into account the poor statistics, consisting of just one object of each type. Expanding the sample of disks seems mandatory to draw more definitive conclusions. It will be also very interesting to observationally locate the snowline of different molecules in the same disk, so that the sequence of snowlines of ices with different binding energies depicted in Fig. 13 can be tracked.

4 Influence of the stellar spectrum and the photodestruction rates

Chemical models of protoplanetary disks contain so many ingredients to deal with the multiple processes at work that the output abundance distributions can be sensitive to many of them. In this study we put the focus on the photochemistry and thus here we evaluate the influence of a couple of related aspects: the spectrum of the star and the way in which photodestruction rates are computed. We concentrate on the T Tauri disk model for this sensitivity analysis.

T Tauri stars are cool, with effective temperatures of the order of 4000 K, although they usually have an important FUV excess that can greatly affect the photochemistry of the disk. To evaluate the influence of this FUV excess we compare our fiducial T Tauri disk model, in which we consider the stellar spectrum of TW Hya, with a model in which we assume that the star emits as a blackbody at a temperature of 4000 K (both spectra are shown in Fig. 1). The lack of FUV excess in this latter case results in much lower photodestruction rates (compare our values in Table B.1 with those of van Dishoeck et al. 2006, or see Heays et al. 2017). The net effect is that without FUV excess, most photodestruction rates are dominated by the ISRF rather than by stellar radiation. As as example, in the left panel of Fig. 14 we

show the photodissociation rate of CO as a function of height at a radius of 1 au, where both the contributions of the ISRF and the star are taken into account. It is seen that in the upper disk, where photodestruction rates are dominated by stellar photons (see Fig. 3), the photodissociation rate of CO in the 4000 K blackbody star model is below that in the fiducial model by many orders of magnitude. A similar behavior occurs for the photodestruction rates of other species. As a consequence, the CO/C/C^+ interface shifts to upper heights and the atomic carbon layer becomes wider (see right panels in Fig. 14). In general, the photochemically active layer, where for example the transition H_2O/OH is located and the radicals C_2H and CN are, is shifted to upper layers. This overall shift of the photochemistry to upper, less dense, and warmer layers, together with the lower strength of the FUV radiation field, induce important changes in the abundances of several molecules. For example, stable molecules like water and the simple organics C_2H_2 and HCN become more abundant at intermediate disk radii compared to the fiducial model (see left panel in Fig. 15), while the radicals C_2H and CN experience a decline in their abundances (see right panel in Fig. 15).

The way in which photodestruction rates are computed may also have an influence on the chemical structure of the photochemically active layer of disks (e.g., Walsh et al. 2012). In our fiducial model, we have used the Meudon PDR code to compute the photodissociation rates of H_2 and CO by solving the excitation and the line-by-line FUV radiative transfer to properly account for self and mutual shielding effects and have computed photodestruction rates for a variety of species using the cross sections compiled in Appendix A. To investigate the effect of using a simpler approach, we have run a T Tauri disk model in which all photodestruction rates are computed through the parametric expression in Eq. (7). The α and γ parameters are taken from Table B.1, while for H_2 and CO we adopt as unattenuated rates and dust shielding factors the values given by Heays et al. (2017). In the left panel of Fig. 14 we compare the resulting CO photodissociation rate as a function of height at a radius of 1 au given by this parametric photodestruction rates approach with that resulting from our fiducial model. It is seen that in the upper disk both approaches yield similar results although at lower heights, where photodestruction is dominated by ISRF photons (see Fig. 3), the parametric approach overestimates the photodissociation rate of CO. The resulting CO/C/C^+ interface is very similar in both scenarios, although it is worth noting that the peak abundance of atomic carbon is lower when the parametric photodestruction rates are used. This has some consequences for the abundances of carbon-bearing species typically formed under the action of photochemistry, such as the radicals C_2H and CN. In fact, these two radicals reach abundances significantly lower in the outer disk when parametric photodestruction rates are used compared to the fiducial model (see right panel in Fig. 15). Other species are also affected to different degrees. For example, while the column density of water does not change much, acetylene becomes less abundant and hydrogen cyanide is slightly enhanced in the range of radii between 1 and 10 au (see left panel in Fig. 15).

5 Conclusions

We have developed a model aimed to compute the chemical composition of a generic protoplanetary disk around a young star. The model considers a passively irradiated disk in steady state and computes the physical and chemical structure of the disk with particular

attention to the disk photochemistry. In particular we have compiled cross sections for 29 molecules and 8 atoms and computed the photodissociation and photoionization rates at each location in the disk by solving the FUV radiative transfer with the Meudon PDR code in a 1+1D approach.

We have applied the model to perform a comparative study of the chemistry of disks around low-mass (T Tauri) and intermediate-mass (Herbig Ae/Be) stars. Infrared and (sub-)mm observations of T Tauri and Herbig disks point to a lower detection rate of molecules in the latter type of disks and, for some species, somewhat lower abundances. Motivated by the observational studies, we have investigated the potential chemical differentiation between disks around these two types of stars, which have very different masses and spectra. We find that globally the chemical behavior of these two types of disks is quite similar, with some important differences driven by the higher stellar ultraviolet flux and the warmer temperatures of Herbig Ae/Be disks.

Water vapor and the simple organic molecules C_2H_2, HCN, and CH_4 are predicted to be very abundant ($\sim 10^{-4}$ for H_2O and a few $\times 10^{-5}$ for the organics) in the hot inner regions of disks around both T Tauri and Herbig Ae/Be stars. The main difference between the two types of disks is that these molecules extend over a larger region in Herbig Ae/Be disks due to the warmer temperatures attained, a finding that is in agreement with the models by Walsh et al. (2015) but in contrast with infrared observations that find a much lower detection rate of water and simple organics toward Herbig Ae/Be disks than toward T Tauri disks. This latter fact is probably caused by observational aspects rather than by substantive differences in the chemistry between these two types of disks. For example, Antonellini et al. (2016) point out that Herbig stars are brighter than T Tauri stars resulting in a higher level of mid-IR continuum and smaller line/continuum ratios. If true, the higher sensitivity and spectral resolution of the James Webb Space Telescope with respect to *Spitzer* could allow to increase the detection rate of water and simple organics in Herbig Ae/Be systems.

Concerning the outer regions of disks, observations point to a lower detection rate of molecules and to somewhat lower abundances in Herbig Ae disks compared to T Tauri disks, although the statistics of Herbig Ae objects observed is small. Our model indicates that in general there are not drastic differences between T Tauri and Herbig Ae disks concerning the abundances of molecules typically observed in disks at (sub-)mm wavelengths. More specifically, various molecules, such as H_2CO, CS, SO, and HCO^+, are observed with similar abundances in the outer regions of T Tauri and Herbig Ae disks and the model satisfactorily finds no clear differentiation between both types of disks for these species. For other species, such as HCN and the radicals C_2H and CN, observations suggest that T Tauri disks may retain somewhat larger abundances than Herbig Ae disks in the outer regions, while the model indeed predicts that these species are slightly less abundant in Herbig Ae disks than in T Tauri disks. In the case of the radicals C_2H and CN, which are produced by the action of photochemistry, the slightly lower abundances calculated in Herbig Ae disks are caused by the higher ultraviolet flux, which narrows the photochemically active layer and limits the ability of photochemistry to synthesize molecules. In any case, for HCN, C_2H, and CN, the observed and calculated abundance differences between both types of disks are small, of a factor of a few at most.

For other organic molecules with a certain complexity such as CH_3OH, HC_3N, CH_3CN, and *c*-C_3H_2, the match with observed values is not satisfactory. This fact, together with the ample dispersion of abundances calculated by different chemical models in the literature point to the chemistry of these molecules not being yet as robust as for simpler species, also because grain-surface chemistry, not included in our model, is likely playing an active role in the synthesis of some of these molecules.

A clear differentiation between T Tauri and Herbig Ae disks is however found concerning ices. The warmer temperatures of Herbig Ae disks shift snowlines to larger radii compared to T Tauri disks and as a consequence disks around intermediate-mass stars are expected to contain a substantially lower mass of ices compared to T Tauri disks.

Supplementary Material

Refer to Web version on PubMed Central for supplementary material.

Acknowledgements

We thank the anonymous referee for a detailed reading and for a constructive report which helped to improve this manuscript. M.A. acknowledges funding support from the European Community 7th Framework Programme through a *Marie Curie Intra-European Individual Fellowship* (grant 235753), from the European Research Council through ERC Synergy grant 610256, and from Spanish MINECO through the Ramón y Cajal programme (RyC-2014-16277) and grant AYA2016-75066-C2-1-P. This work was partly supported by the CNRS program *Physique et Chimie du Milieu Interstellaire* (PCMI) co-funded by the Centre National d'Études Spatiales (CNES). We thank J. R. Goicoechea, E. Bron, S. Cazaux, G. M. Muñoz-Caro, R. Martín-Doménech, and A. Fuente for useful discussions, S. Miyake for help in the treatment of cross sections from the former version of the Leiden database, and E. A. Bergin, C. E. Brion, J. A. Nuth, D. M. P. Holland, K.-L. Han, and J.-H. Fillion for kindly providing useful data.

References

Aguado A, Roncero O, Zanchet A, et al. ApJ. 2017; 838:33.
Agúndez M, Cernicharo J. ApJ. 2006; 650:374.
Agúndez M, Cernicharo J, Goicoechea JR. A&A. 2008; 483:831.
Agúndez M, Goicoechea JR, Cernicharo J, et al. ApJ. 2010; 713:662.
Agúndez M, Wakelam V. Chem Rev. 2013; 113:8710. [PubMed: 24099569]
Aikawa Y, Miyama SM, Nakano T, Umebayashi T. ApJ. 1996; 467:684.
Aikawa Y, Umebayashi T, Nakano T, Miyama SM. ApJ. 1997; 486:L51.
Aikawa Y, Umebayashi T, Nakano T, Miyama SM. ApJ. 1999; 519:705.
Aikawa Y, Herbst E. ApJ. 1999a; 526:314.
Aikawa Y, Herbst E. A&A. 1999b; 351:233.
Aikawa Y, Herbst E. A&A. 2001; 371:1107.
Aikawa Y, van Zadelhoff GJ, van Dishoeck EF, Herbst E. A&A. 2002; 622:632.
Aikawa Y, Momose M, Thi W-F, et al. PASJ. 2003; 55:11.
Aikawa Y, Nomura H. ApJ. 2006; 642:1152.
Aikawa Y. ApJ. 2007; 656:L93.
Akimkin V, Zhukovska S, Wiebe D, et al. ApJ. 2013; 766:8.
Albertsson T, Semenov D, Henning Th. ApJ. 2014; 784:39.
Andersson S, van Dishoeck EF. A&A. 2008; 491:907.
Anicich VG. JPL Publication 03-19. 2003
Antonellini S, Kamp I, Lahuis F, et al. A&A. 2016; 585:A61.

Apaydin G, Fink WH, Jackson WM. J Chem Phys. 2004; 121:9368. [PubMed: 15538856]
Aresu G, Kamp I, Meijerink R, et al. A&A. 2011; 526:A163.
Arthur NL. J Chem Soc, Faraday Trans 2. 1986; 82:331.
Attard G, Barnes C. Surfaces. Oxford Science Publications; 1998. 72
Atkinson R, Baulch DL, Cox RA, et al. Atm Chem Phys. 2004; 4:1461.
Atkinson R, Baulch DL, Cox RA, et al. Atm Chem Phys. 2006; 6:3625.
Au JW, Cooper G, Burton GR, et al. Chem Phys. 1993; 173:209.
Ayres TR. ApJS. 2010; 187:149.
Banzatti A, Pontoppidan KM, Salyk C, et al. ApJ. 2017; 834:152.
Barsuhn J, Nesbet RK. J Chem Phys. 1978; 68:2783.
Bast JE, Lahuis F, van Dishoeck EF, Tielens AGGM. A&A. 2013; 551:A118.
Baulch DL, Bowman CT, Cobos CJ, et al. J Phys Chem Ref Data. 2005; 34:757.
Bergin E, Calvet N, D'Alessio P, Herczeg GJ. ApJ. 2003; 591:L159.
Bergin EA, Aikawa Y, Blake GA, van Dishoeck EF. Protostars and Planets V. Reipurth B, Jewitt D, Keil K, editorsUniversity Arizona Press; 2007. 751951
Bergin EA, Hogerheijde MR, Brinch C, et al. A&A. 2010; 521:L33.
Bergin EA, Du F, Cleeves LI, et al. ApJ. 2016; 831:101.
Bertin M, Fayolle EC, Romanzin C, et al. Phys Chem Chem Phys. 2012; 14:9929. [PubMed: 22710615]
Bertin M, Fayolle EC, Romanzin C, et al. ApJ. 2013; 779:120.
Bertin M, Romanzin C, Doronin M, et al. ApJ. 2016; 817:L12.
Bethell T, Bergin E. Science. 2009; 326:1675. [PubMed: 20019283]
Biehl H, Schönnenbeck G, Stuhl F, Staemmler V. J Chem Phys. 1994; 101:3819.
Blevins SM, Pontoppidan KM, Banzatti A, et al. ApJ. 2016; 818:22.
Brion CE, Dyck M, Cooper G. J Electron Spectrosc Relat Phenom. 2005; 144:127.
Bron E, Le Bourlot J, Le Petit F. A&A. 2014; 569:A100.
Bruna PJ, Kammer WE, Vasudevan K. Chem Phys. 1975; 9:91.
Bruna PJ, Hirsch G. Mol Physics. 1987; 61:1359.
Burcat A, Ruscic B. ANL-05/20 and TAE 960 Technion-IIT. 2005
Burton GR, Chan WF, Cooper G, Brion CE. Chem Phys. 1993; 177:217.
Burke DJ, Brown WA. Phys Chem Chem Phys. 2010; 12:5947. [PubMed: 20520900]
Callear AB, Metcalfe P. Chem Phys. 1976; 14:275.
Cameron M, Sivakumaran V, Dillon TJ, Crowley JN. Phys Chem Chem Phys. 2002; 4:3628.
Carney MT, Hogerheijde MR, Loomis RA. A&A. 2017; 605:A21.
Carr JS, Tokunaga AT, Najita J. ApJ. 2004; 603:213.
Carr JS, Najita JR. Science. 2008; 319:1504. [PubMed: 18339932]
Carr JS, Najita JR. ApJ. 2011; 733:102.
Carr JS, Najita JR. ApJ. 2014; 788:66.
Castelli F, Kurucz RL. arXiv:astro-ph/0405087. 2004
Cazaux S, Tielens AGGM. ApJ. 2002a; 575:L29.
Cazaux S, Tielens AGGM. ApJ. 2002b; 577:L127.
Ceccarelli C, Dominik C, Lefloch B, et al. ApJ. 2004; 607:L51.
Cernicharo J. ApJ. 2004; 608:L41.
Chaabouni H, Bergeron H, Baouche S, et al. A&A. 2012; 538:A128.
Chan WF, Cooper G, Brion CE. Chem Phys. 1993a; 178:387.
Chan WF, Cooper G, Brion CE. Chem Phys. 1993b; 170:99.
Chan WF, Cooper G, Sodhi RNS, Brion CE. Chem Phys. 1993c; 170:81.
Chapillon E, Guilloteau S, Dutrey A, et al. A&A. 2012a; 537:A60.
Chapillon E, Dutrey A, Guilloteau S, et al. ApJ. 2012b; 756:58.

Chen B-M, Lu H-C, Chen H-K, et al. ApJ. 2006a; 647:1535.
Chen S, Zhou W, Zhang J. Chem Phys Lett. 2006b; 418:328.
Chenel A, Roncero O, Aguado A, et al. J Chem Phys. 2016; 144 144306.
Cleeves LI, Bergin EA, Qi C, et al. ApJ. 2015; 799:204.
Collings MP, Anderson MA, Chen R, et al. MNRAS. 2004; 354:1133.
Cook PA, Langford SR, Dixon RN, Ashfold MNR. J Chem Phys. 2001; 114:1672.
Cooper G, Burton GR, Brion CE. J Electron Spectrosc Relat Phenom. 1995; 73:139.
Cooper G, Anderson JE, Brion CE. Chem Phys. 1996; 209:61.
Crovisier J. A&A. 1989; 213:459.
Cruz-Diaz GA, Martín-Doménech R, Muñoz Caro GM, Chen Y-J. A&A. 2016; 592:A68.
Cunto W, Mendoza C, Ochsenbein F, Zeippen CJ. A&A. 1993; 275:L5.
Cuppen HM, Walsh C, Lamberts T, et al. Space Sci Rev. 2017; 212:1.
Daviel S, Iida Y, Carnovale F, Brion CE. Chem Phys. 1984; 83:319.
Dehmer PM. Chem Phys Lett. 1984; 110:79.
Dominik C, Ceccarelli C, Hollenbach D, Kaufman M. ApJ. 2005; 635:L85.
Doppmann GW, Najita JR, Carr JS, Graham JR. ApJ. 2011; 738:112.
Doronin M, Bertin M, Michaut X, et al. J Chem Phys. 2015; 143 084703.
Draine BT. ApJS. 1978; 36:595.
Draine BT, Lee HM. ApJ. 1984; 285:89.
Driscoll JN, Warneck P. J Phys Chem. 1968; 72:3736.
Du F, Bergin EA. ApJ. 2014; 792:2.
Du F, Bergin EA, Hogerheijde M, et al. ApJ. 2017; 842:98.
Duflot D, Robbe J-M, Flament J-P. J Chem Phys. 1994; 100:1236.
Dullemond CP, Dominik C. A&A. 2004; 417:159.
Dutrey A, Guilloteau S, Guélin M. A&A. 1997; 317:L55.
Dutrey A, Henning T, Guilloteau S, et al. A&A. 2007; 464:615.
Dutrey A, Wakelam V, Boehler Y, et al. A&A. 2011; 535:A104.
Dutrey A, Semenov D, Chapillon E. , et al. Protostars and Planets VI. Beuther H, Klessen RS, Dullemond CP, Henning T, editorsVol. 914. University Arizona Press; 2014. 317
Edvardsson D, Battzer P, Karlsson L, et al. J Phys B: At Mol Opt Phys. 1999; 32:2583.
Fayolle EC, Bertin M, Romanzin C, et al. ApJ. 2011; 739:L36.
Fayolle EC, Bertin M, Romanzin C, et al. A&A. 2013; 556:A122.
Fayolle EC, Balfe J, Loomis R, et al. ApJ. 2016; 816:L28.
Fedele D, Pascucci I, Brittain S, et al. ApJ. 2011; 732:106.
Fedele D, Bruderer S, van Dishoeck EF, et al. A&A. 2012; 544:L9.
Fedele D, Bruderer S, van Dishoeck EF, et al. A&A. 2013; 559:A77.
Feng R, Cooper G, Brion CE. Chem Phys. 1999a; 127:142.
Feng R, Cooper G, Brion CE. Chem Phys. 1999b; 249:223.
Feng R, Cooper G, Burton GR, et al. Chem Phys. 1999c; 240:371.
Fillion J-H, Dulieu F, Baouche S, et al. J Phys B: At Mol Opt Phys. 2003; 36:2767.
Fillion J-H, Ruiz J, Yang X-F, et al. J Chem Phys. 2004; 120:6531. [PubMed: 15267544]
Fillion J-H, Fayolle EC, Michaut X, et al. Faraday Discuss. 2014; 168:533. [PubMed: 25302397]
Fitzpatrick EL, Massa D. ApJ. 2007; 663:320.
Florescu-Mitchell AI, Mitchell JBA. Phys Rep. 2006; 430:277.
Fogel JKJ, Bethell TJ, Bergin EA, et al. ApJ. 2011; 726:29.
France K, Schindhelm E, Herczeg GJ, et al. ApJ. 2012; 756:171.
France K, Schindhelm E, Bergin EA, et al. ApJ. 2014; 784:127.
Fraser HJ, Collings MP, McCoustra MRS, Williams DA. MNRAS. 2001; 327:1165.
Fuente A, Cernicharo J, Agúndez M, et al. A&A. 2010; 524:A19.

Fuente A, Cernicharo J, Agúndez M. ApJ. 2012; 754:L6.
Furuya K, Nomura Y, Hersant F, Wakelam V. ApJ. 2013; 779:11.
Gans B, Vieira Mendes LA, Boyé-Péronne S, et al. J Phys Chem A. 2010; 114:3237. [PubMed: 19947606]
Gans B, Boyé-Péronne S, Broquier M, et al. Phys Chem Chem Phys. 2011; 13:8140. [PubMed: 21340077]
Garrod RT, Herbst E. A&A. 2006; 457:927.
Geppert WD, Larsson M. Mol Physics. 2008; 106:16.
Gibb EL, van Brunt KA, Brittain SD, Rettig TW. ApJ. 2007; 660:1572.
Gibb EL, Horne D. ApJ. 2013; 776:L28.
Gibson ST, Greene JP, Berkowitz J. J Chem Phys. 1985; 83:4319.
Glassgold AE, Najita JR, Igea J. ApJ. 2004; 615:972.
Glassgold AE, Meijerink R, Najita JR. ApJ. 2009; 701:142.
Goicoechea JR, Le Bourlot J. A&A. 2007; 467:1.
González García M, Le Bourlot J, Le Petit F, Roueff E. A&A. 2008; 485:127.
Goumans TPM, Richard C, Catlow A, Brown WA. MNRAS. 2009; 393:1403.
Graedel TE, Langer WD, Frerking MA. ApJS. 1982; 48:321.
Graninger D, Öberg KI, Qi C, Kastner J. ApJ. 2015; 807:L15.
Gredel R, Lepp S, Dalgarno A, Herbst E. ApJ. 1989; 347:289.
Groth WE, Schurath U, Schindler RN. J Phys Chem. 1968; 72:3914.
Guest JA, Lee LC. J Phys B: At Mol Opt Phys. 1981; 14:3401.
Guilloteau S, Piétu V, Dutrey A, Guélin M. A&A. 2006; 448:L5.
Guilloteau S, Dutrey A, Wakelam V, et al. A&A. 2012; 548:A70.
Guilloteau S, Di Folco E, Dutrey A, et al. A&A. 2013; 549:A92.
Guilloteau S, Reboussin L, Dutrey A, et al. A&A. 2016; 592:A124.
Habing HJ. Bull Astron Inst Netherlands. 1968; 19:421.
Harada N, Herbst E, Wakelam V. ApJ. 2010; 721:1570.
Hartquist TW, Williams DA. MNRAS. 1990; 247:343.
Hasegawa TI, Herbst E, Leung CM. ApJS. 1992; 82:167.
Hasegawa TI, Herbst E. MNRAS. 1993; 261:83.
Heays AN, Bosman AD, van Dishoeck EF. A&A. 2017; 602:A105.
Heinzeller D, Nomura H, Walsh C, Millar TJ. 2011; 731:115.
Henning ThSemenov D, Guilloteau S. , et al. ApJ. 2010; 714:1511.
Henning ThSemenov D. Chem Rev. 2013; 113:9016. [PubMed: 24191756]
Herczeg GJ, Valenti JA, Johns-Frull CM, Wood BE. ApJ. 2002; 572:310.
Herzberg G. Proc Roy Soc London Ser A. 1961; 262:291.
Hily-Blant P, Magalhaes V, Kastner J, et al. A&A. 2017; 603:L6.
Hogerheijde MR, Bergin EA, Brinch C, et al. Science. 2011; 334:338. [PubMed: 22021851]
Holland DMP, Shaw DA, McSweeney SM, et al. Chem Phys. 1993; 173:315.
Holland DMP, Shaw DA, Hayes MA. Chem Phys. 1995; 201:299.
Hollenbach D, Kaufman MJ, Bergin EA, Melnick GJ. ApJ. 2009; 690:1497.
Huang J, Öberg KI. ApJ. 2015; 809:L26.
Huang J, Öberg KI, Qi C, et al. ApJ. 2017; 835:231.
Hudson RD. Rev Geophys Space Phys. 1971; 9:305.
Huebner WF, Keady JJ, Lyon SP. Ap&SS. 1992; 195:1.
Huestis DL, Berkowitz J. BAAS. 2010; 42:972.
Hughes KJ, Turányi T, Clague AR, Pilling MJ. Int J Chem Kinet. 2001; 33:513.
Ilgner M, Henning Th, Markwick AJ, Millar TJ. A&A. 2004; 415:643.
Ilgner M, Nelson RP. A&A. 2006a; 445:731.

Ilgner M, Nelson RP. A&A. 2006b; 445:223.
Ilgner M, Nelson RP. A&A. 2006c; 445:205.
Ingleby L, Calvet N, Bergin E, et al. ApJ. 2009; 703:L137.
Janssen LMC, van der Loo MPJ, Groenenboom GC, et al. J Chem Phys. 2007; 126:94304.
Jonkheid B, Dullemond CP, Hogerheijde MR, van Dishoeck EF. A&A. 2007; 463:203.
Jura M. ApJ. 1975; 197:575.
Kamp I, Dullemond CP. ApJ. 2004; 615:991.
Kamp I, Thi W-F, Woitke P, et al. A&A. 2017; 607:A41.
Kassner ChStuhl F. Chem Phys Lett. 1994; 222:425.
Kastner JH, Hily-Blant P, Rodriguez DR, et al. ApJ. 2014; 793:55.
Kenyon SJ, Hartmann L. ApJS. 1995; 101:117.
Khamaganov V, Karunanandan R, Rodriguez A, Crowley JN. Phys Chem Chem Phys. 2007; 9:4098. [PubMed: 17687461]
Koch A. J Phys Chem A. 1997; 101:1460.
Konnov AA. Detailed reaction mechanism for small hydrocarbon combustion, Release 0.5. 2000
Kruger AJ, Richter MJ, Carr JS, et al. ApJ. 2011; 729:145.
Kastner JH, Zuckerman B, Weintraub DA, Forveille T. Science. 1997; 277:67. [PubMed: 9204898]
Kastner JH, Hily-Blant P, Rodriguez DR, et al. ApJ. 2014; 793:55.
Kirby K, Roberge WG, Saxon RP, Liu B. ApJ. 1980; 239:855.
Kirby K, Goldfield EM. J Chem Phys. 1991; 94:1271.
Kroes G-J, van Hemert MC, Billing GD, Neuhauser D. J Chem Phys. 1997; 107:5757.
Lahuis F, van Dishoeck EF, Boogert ACA, et al. ApJ. 636:L145.
Laor A, Draine BT. ApJ. 1993; 402:441.
Lavendy H, Robbe JM, Gandara G. J Phys B: At Mol Opt Phys. 1987; 20:3067.
Le Bourlot J, Pineau des Forêts G, Roueff E, Flower DR. A&A. 1995; 302:870.
Le Bourlot J, Le Petit F, Pinto C, et al. A&A. 2012; 541:A76.
Le Petit FL, Nehmé C, Le Bourlot J, Roueff E. ApJS. 2006; 164:506.
Lee H-H, Roueff E, Pineau des Forêts G, et al. A&A. 1998; 334:1047.
Léger A, Jura M, Omont A. A&A. 1985; 144:147.
Li Y-J, Zhang P-Y, Han K-L. J Mol At Sci. 2010; 1:18.
Lide RD. CRC Handbook of Chemistry and Physics. 90th ed. CRC Press; 2009.
Lilly RL, Rebbert RE, Ausloos P. J Photochem. 1973; 2:49.
Litorja M, Ruscic B. J Chem Phys. 1998; 108:6748.
Loison J-C. J Phys Chem A. 2010; 114:6515. [PubMed: 20491459]
Loomis RA, Cleeves LI, Öberg KI, et al. ApJ. 2015; 809:L25.
Luna R, Satorre MÁ, Santonja C, Domingo M. A&A. 2014; 566:A27.
Macpherson MT, Pilling MJ, Smith MJC. J Phys Chem. 1985; 89:2268.
Maergoiz AI, Nikitin EE, Troe J. Int J Mass Spectrom. 2009; 280:42.
Markwick AJ, Ilgner M, Millar TJ, Henning Th. A&A. 2002; 385:632.
Martín-Doménech R, Muñoz Caro GM, Bueno J, Goesmann F. A&A. 2014; 564:A8.
Martín-Doménech R, Manzano-Santamaría J, Muñoz Caro, et al. A&A. 2015; 584:A14.
Martin-Zaïdi C, Deleuil M, Le Bourlot J, et al. A&A. 2008; 484:225.
Mamajek EE. ApJ. 2005; 634:1385.
Manatt SL, Lane AL. J Quant Spec Radiat Transf. 1993; 50:267.
Mandell AM, Mumma MJ, Blake GA, et al. ApJ. 2008; 681:L25.
Mandell AM, Bast J, van Dishoeck EF, et al. ApJ. 747:92.
Manion JA, Huie RE, Levin RD, et al. NIST Chemical Kinetics Database, Data version 2013.03. 2013
Mathews GS, Klaassen PD, Juhász A, et al. A&A. 2013; 557:A132.
Mathis JS, Rumpl W, Nordsieck KH. ApJ. 1977; 217:425.

Mathis JS, Mezger PG, Panagia N. A&A. 1983; 128:212.
McBride BJ, Zehe MJ, Gordon S. NASA Report TP-2002-211556. 2002
McElroy D, Walsh C, Markwick AJ, et al. A&A. 2013; 550:A36.
McMillan EC, Shen G, McCann JF, et al. J Phys B: At Mol Opt Phys. 2016; 49:084001.
McNesby JR, Tanaka I, Okabe H. J Chem Phys. 1962; 36:605.
Mebel AM, Hayashi M, Jackson WM, et al. J Chem Phys. 2001; 114:9821.
Meeus G, Montesinos B, Mendigutía I, et al. A&A. 2012; 544:A78.
Mentall JE, Gentieu EP, Krauss M, Neumann D. J Chem Phys. 1971; 55:5471.
Montesinos B, Eiroa C, Mora A, Merín B. A&A. 2009; 495:901.
Mota R, Parafita R, Giuliani A, et al. Chem Phys Lett. 2005; 416:152.
Muñoz Caro GM, Jiménez-Escobar A, Martín-Gago JÁ, et al. A&A. 2010; 522:A108.
Najita JR, Carr JS, Strom SE, et al. ApJ. 2010; 712:274.
Najita JR, Carr JS, Pontoppidan KM, et al. ApJ. 2013; 766:134.
Nee JB, Suto M, Lee LC. J Phys B: At Mol Opt Phys. 1985; 18:L293.
Nee JB, Lee JC. J Chem Phys. 1984; 81:31.
Nee JB, Lee LC. J Chem Phys. 1986; 84:5303.
Neufeld DA, Wolfire MG. ApJ. 2009; 706:1594.
Noble JA, Congiu E, Dulieu F, Fraser HJ. MNRAS. 2012a; 421:768.
Noble JA, Theule P, Mispelaer F, et al. A&A. 2012b; 543:A5.
North SW, Blank DA, Chu PM, Lee YT. J Chem Phys. 1995; 102:792.
Norwood K, Ng CY. Chem Phys Lett. 1989; 156:145.
Norwood K, Nourbakhsh S, He G-H, Ng CY. Chem Phys Lett. 1991; 184:147.
Nuth JA, Glicker S. J Quant Spec Radiat Transf. 1982; 28:223.
Öberg KI, Linnartz H, Visser R, van Dishoeck EF. ApJ. 2009; 693:1209.
Öberg KI, Qi C, Fogel JKJ, et al. ApJ. 2010; 720:480.
Öberg KI, Qi C, Fogel JKJ, et al. ApJ. 2011; 734:98.
Öberg KI, Guzmán VV, Furuya K, et al. Nature. 2015; 520:198. [PubMed: 25855455]
Öberg KI, Guzmán VV, Merchant CJ, et al. ApJ. 2017; 839:43.
Okabe H, Lenzi M. J Chem Phys. 1967; 47:5241.
Pacheco-Vázquez S, Fuente A, Agúndez M, et al. A&A. 2015; 578:A81.
Pacheco-Vázquez S, Fuente A, Baruteau C. A&A. 2016; 589:A60.
Pascucci I, Herczeg G, Carr JS, Bruderer S. ApJ. 2013; 779:178.
Phillips LF. J Phys Chem. 1981; 85:3994.
Piétu V, Dutrey A, Guilloteau S. A&A. 2007; 467:163.
Podio L, Kamp I, Codella C, et al. ApJ. 2013; 766:L5.
Pontoppidan KM, Salyk C, Blake GA, et al. ApJ. 2010a; 720:887.
Pontoppidan KM, Salyk C, Blake GA, Käufl HU. ApJ. 2010b; 722:L173.
Pontoppidan KM, Salyk C, Bergin EA. , et al. Protostars and Planets VI. Beuther H, Klessen RS, Dullemond CP, Henning T, editorsVol. 914. University Arizona Press; 2014. 363
Pouilly B, Robbe JM, Schamps J, Roueff E. J Phys B: At Mol Opt Phys. 1983; 16:437.
Prasad SS, Tarafdar SP. ApJ. 1983; 267:603.
Qi C, Kessler JE, Koerner DW, et al. ApJ. 2003; 597:986.
Qi C, Wilner DJ, Aikawa Y, et al. ApJ. 2008; 681:1396.
Qi C, Öberg KI, Wilner DJ. ApJ. 2013a; 765:34.
Qi C, Öberg KI, Wilner DJ, Rosenfeld KA. ApJ. 2013b; 765:L14.
Qi C, Öberg KI, Wilner DJ, et al. Science. 2013c; 341:630. [PubMed: 23868917]
Qi C, Öberg KI, Andrews SM, et al. ApJ. 2015; 813:128.
Riviere-Marichalar P, Ménard F, Thi W-F, et al. A&A. 2012; 538:L3.
Roberge WG, Jones D, Lepp S, Dalgarno A. ApJS. 1991; 77:287.

Roberge A, Lecavelier des Etangs A, Grady CA, et al. ApJ. 2001; 551:L97.
Roueff E, Alekseyev AB, Le Bourlot J. A&A. 2014; 566:A30.
Ruscic B, Berkowitz J. Phys Rev Lett. 1983; 50:675.
Salinas VN, Hogerheijde MR, Bergin EA, et al. A&A. 2016; 591:A122.
Salyk C, Blake GA, Boogert ACA, Brown JM. ApJ. 2007; 655:L105.
Salyk C, Pontoppidan KM, Blake GA, et al. ApJ. 2008; 676:L49.
Salyk C, Pontoppidan KM, Blake GA, et al. ApJ. 2011; 731:130.
Sander SPJ, Abbatt JR, Barker JB. , et al. JPL Publication; 2011. 10–6.
Sandford SA, Allamandola LJ. ApJ. 1993; 417:815.
Sargent BA, Forrest W, Watson DM, et al. ApJ. 2014; 792:83.
Sarrasin E, Abdalah DB, Wernli M, et al. MNRAS. 2010; 404:518.
Semenov D, Wiebe D, Henning Th. A&A. 2004; 417:93.
Semenov D, Wiebe D, Henning Th. ApJ. 2006; 647:L57.
Semenov D, Wiebe D. ApJS. 2011; 196:25.
Schreyer K, Guilloteau S, Semenov D, et al. A&A. 2008; 491:821.
Schriver-Mazzuoli L, Chaabouni H, Schriver A. J Mol Struct. 2003; 644:151.
Schwarz KR, Bergin EA, Cleeves LI, et al. ApJ. 2016; 823:91.
Shen CJ, Greenberg JM, Schutte WA, van Dishoeck EF. A&A. 2004; 415:203.
Slanger TG, Black G. J Chem Phys. 1982; 77:2432.
Smith IWM, Sage AM, Donahue NM, et al. Faraday Discuss. 2006; 133:137. [PubMed: 17191447]
Sorkhabi O, Blunt VM, Lin H, et al. J Chem Phys. 1997; 107:9842.
Stephens JA, McKoy V. J Chem Phys. 1988; 88:1737.
Stark G, Yoshino K, Smith PL. J Mol Spectr. 1987; 124:420.
Stief LJ, Donn B, Glicker S, et al. ApJ. 1972; 171:21.
Su T, Chesnavich WJ. J Chem Phys. 1982; 76:5183.
Teague R, Semenov D, Guilloteau S, et al. A&A. 2015; 574:A137.
Taatjes CA, Osborn DL, Selby TM, et al. J Phys Chem A. 2008; 112:9336. [PubMed: 18572896]
Telleschi A, Güdel M, Briggs KR, et al. A&A. 2007; 468:541.
Thi W-F, van Zadelhoff G-J, van Dishoeck EF. A&A. 2004; 425:955.
Thi W-F, Woitke P, Kamp I. MNRAS. 2010; 407:232.
Thi W-F, Ménard F, Meeus G, et al. A&A. 2011; 530:L2.
Toffoli D, Lucchese RR. J Chem Phys. 2004; 120:6010. [PubMed: 15267483]
van Dishoeck EF, Dalgarno A. ApJ. 1984; 277:576.
van Dishoeck EF. J Chem Phys. 1987; 86:196.
van Dishoeck EF, Beärda RA, van Hemert MC. A&A. 1996; 307:645.
van Dishoeck EF, Thi W-F, van Zadelhoff G-J. A&A. 2003; 400:L1.
van Dishoeck EF, Jonkheid B, van Hemert MC. Faraday Discuss. 2006; 133:231. [PubMed: 17191450]
van Dishoeck EF, Bergin EA, Lis DC, Lunine JI. Protostars and Planets VI. Beuther H, Klessen RS, Dullemond CP, Henning T, editorsVol. 835. University Arizona Press; 2014. 914
van Hemert MC, van Dishoeck EF. Chem Phys. 2008; 343:292.
van Zadelhoff G-J, van Dishoeck EF, Thi W-F, Blake GA. A&A. 2001; 377:566.
van Zadelhoff G-J, Aikawa Y, Hogerheijde MR, van Dishoeck EF. A&A. 2003; 397:789.
Vasyunin AI, Semenov D, Henning Th, et al. ApJ. 2008:672.
Venot O, Fray N, Bénilan Y, et al. A&A. 2013; 551:A131.
Verner DA, Ferland GJ, Korista KT, Yakovlev DG. ApJ. 1996; 465:487.
Vetter R, Zülicke L, Koch A, et al. J Chem Phys. 1996; 104:5558.
Wakelam V, Smith IWM, Herbst E, et al. Space Sci Rev. 2010; 156:13.
Wakelam V, Herbst E, Loison J-C, et al. ApJS. 2012; 199:21.
Wakelam V, Loison J-C, Herbst E, et al. ApJS. 2015; 217:20.

Walsh C, Millar TJ, Nomura H. ApJ. 2010; 722:1607.
Walsh C, Nomura H, Millar TJ, Aikawa Y. ApJ. 2012; 747:114.
Walsh C, Millar TJ, Nomura H, et al. A&A. 2014; 563:A33.
Walsh C, Nomura H, van Dishoeck E. A&A. 2015; 582:A88.
Walsh C, Loomis RA, Öberg KI, et al. ApJ. 2016; 823:L10.
Webb RA, Zuckerman B, Platais I, et al. ApJ. 1999; 512:L63.
Wang K, Stephens JA, McKoy V. J Chem Phys. 1990; 93:7874.
Wang J, Yang B, Cool TA, et al. Int J Mass Spectrom. 2008; 269:210.
Watanabe K, Matsunaga FM, Sakai H. Appl Opt. 1967; 6:391. [PubMed: 20057764]
Weingartner JC, Draine BT. ApJ. 2001; 548:296.
Wheeler MD, Orr-Ewing AJ, Ashfold MNR. J Chem Phys. 1997; 107:7591.
Willacy K, Khlar HH, Millar TJ, Henning Th. A&A. 1998; 338:995.
Willacy K, Langer WD. ApJ. 2000; 544:903.
Willacy K, Langer W, Allen M, Bryden G. ApJ. 2006; 644:1202.
Willacy K. ApJ. 2007; 660:441.
Willacy K, Woods PM. ApJ. 2009; 703:479.
Wilson SHS, Howe JD, Rosser KN, et al. Chem Phys Lett. 1994; 227:456.
Woitke P, Kamp I, Thi W-F. A&A. 2009; 501:383.
Woitke P, Min M, Pinte C, et al. A&A. 2016; 586:A103.
Woodall J, Agúndez M, Markwick-Kemper AJ, Millar TJ. A&A. 2007; 466:1197.
Woods PM, Willacy K. ApJ. 2007; 655:L49.
Wu CYR, Yang BW, Chen FZ, et al. Icarus. 2000; 145:289.
Wu G, Jiang B, Ran Q, et al. J Chem Phys. 2004; 120:2193. [PubMed: 15268357]
Wu Y-J, Lu H-C, Chen H-K, et al. J Chem Phys. 2007; 127:154311. [PubMed: 17949153]
Yang L, Ciesla FJ, Alexander CMO'D. Icarus. 2013; 226:256.
Yoshino K, Parkinson WH, Ito K, Matsui T. J Mol Spectr. 2005; 229:238.
Zanchet A, Agúndez M, Herrero VJ, et al. AJ. 2013; 146:125.
Zhang K, Bergin EA, Blake GA, et al. Nature Astron. 2017; 1:0130.

Europe PMC Funders Author Manuscripts

Europe PMC Funders Author Manuscripts

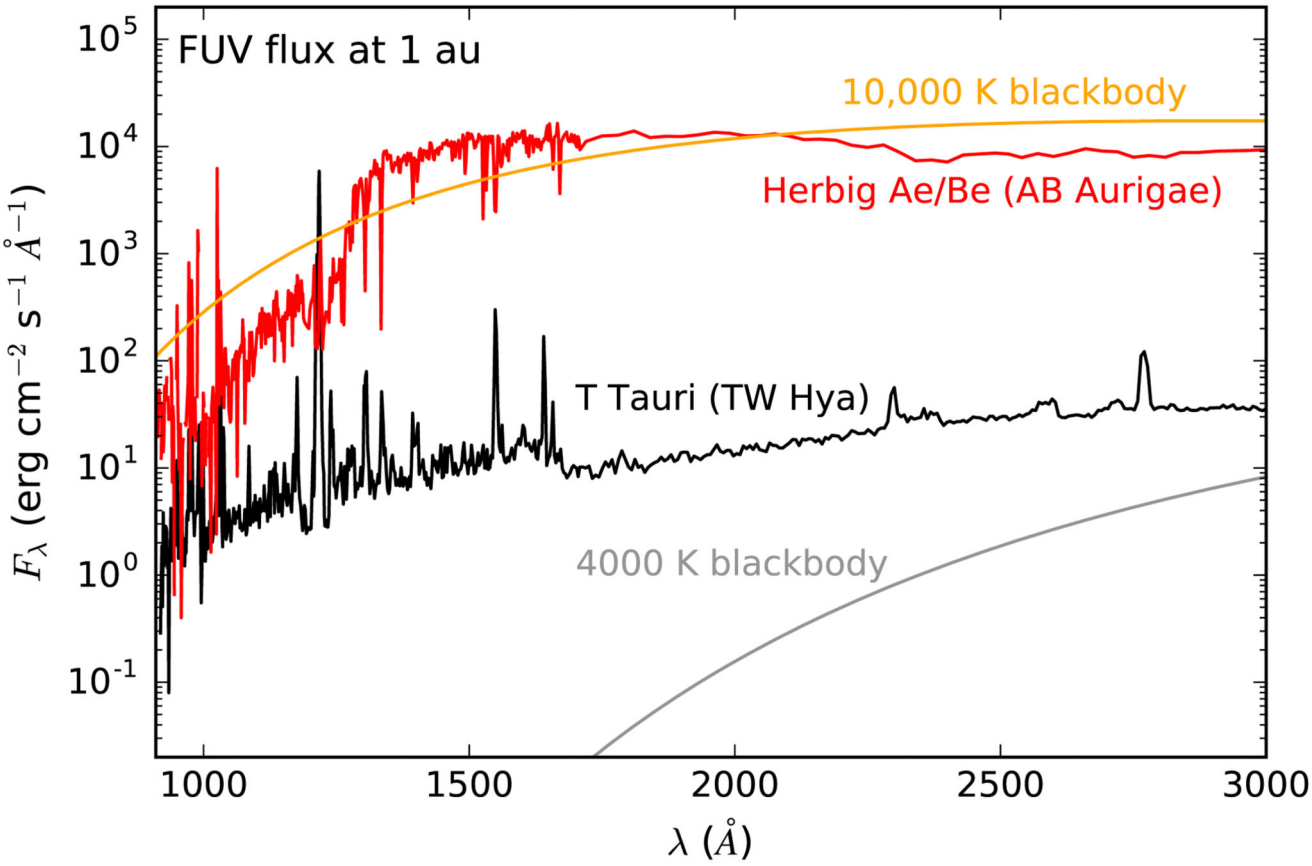

Fig. 1.

Stellar FUV flux at 1 au of the T Tauri star (emitting as TW Hya and as a 4000 K blackbody) and of the Herbig Ae/Be star (emitting as AB Aurigae and as a 10,000 K blackbody).

Europe PMC Funders Author Manuscripts

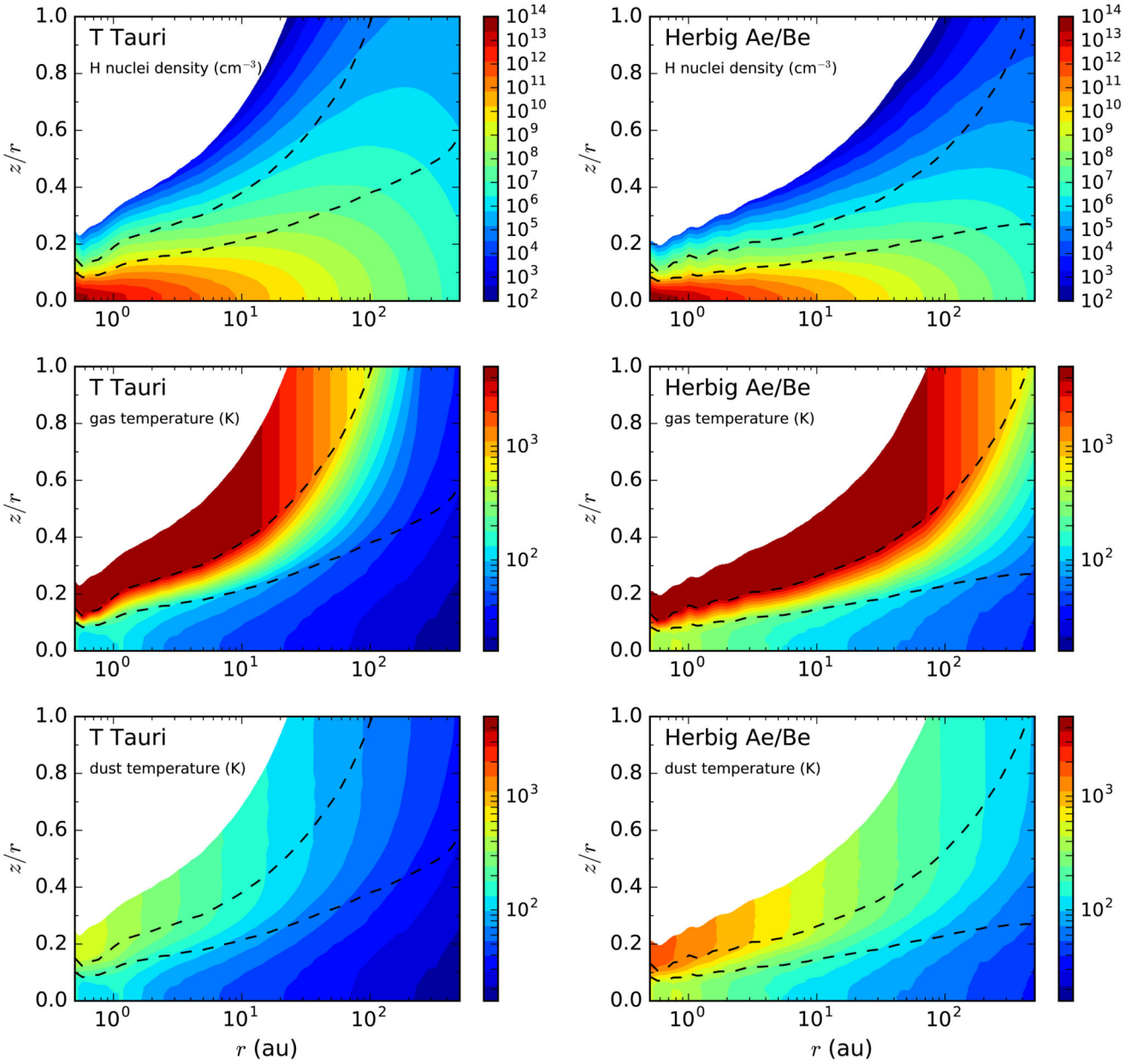

Fig. 2.

Calculated volume density of H nuclei (top), gas temperature (middle), and dust temperature (bottom) as a function of radius r and height over radius z/r for the T Tauri (left) and Herbig Ae/Be (right) disks. The dashed lines indicate the location where A_V in the outward vertical direction takes values of 0.01 and 1.

Europe PMC Funders Author Manuscripts

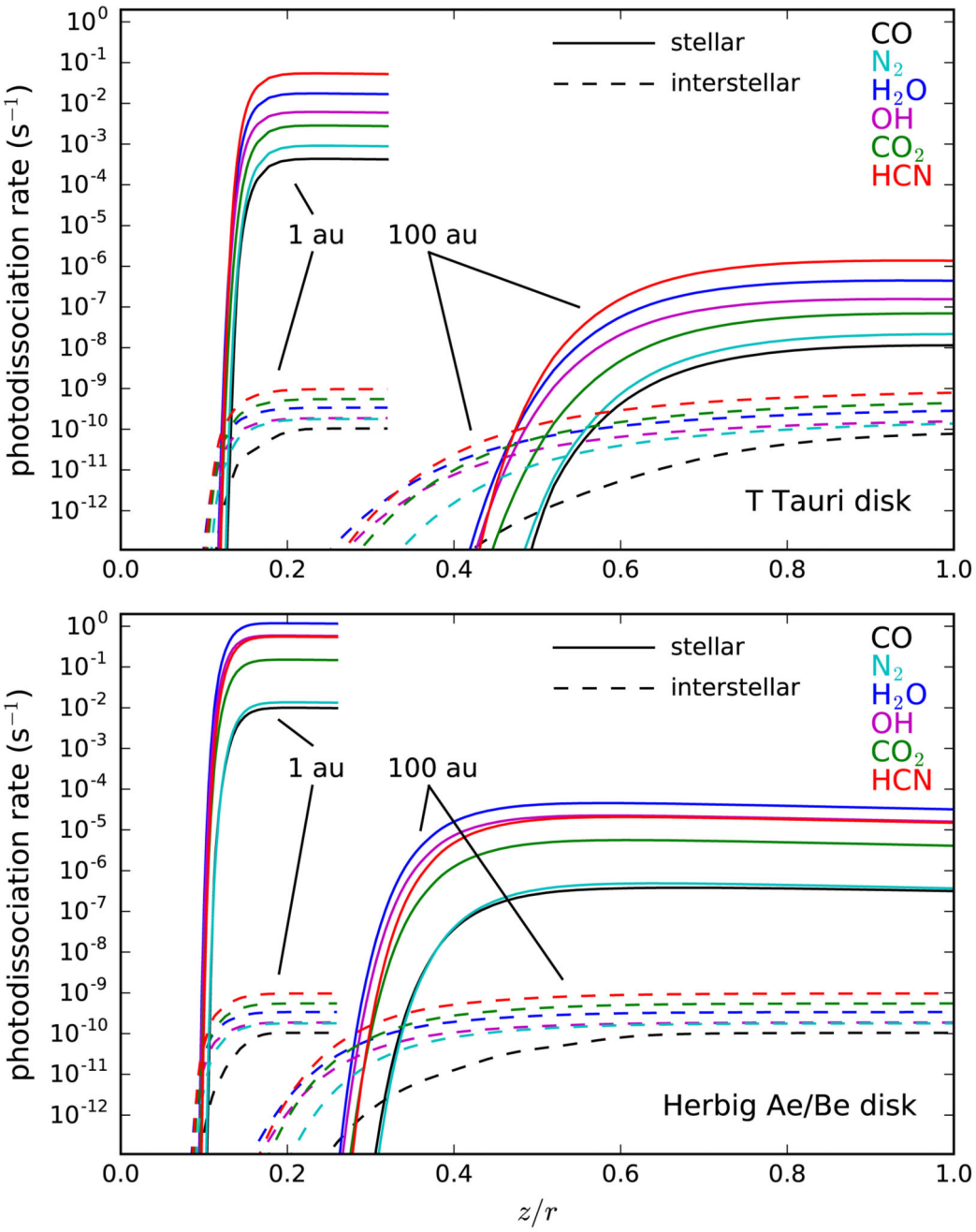

Fig. 3.

Contribution of the stellar (solid lines) and interstellar (dashed lines) FUV fields to the photodissociation rates of various molecules as a function of the height over radius (*z*/*r*) at 1 au and 100 au in the T Tauri (upper panel) and Herbig Ae/Be (lower panel) disks.

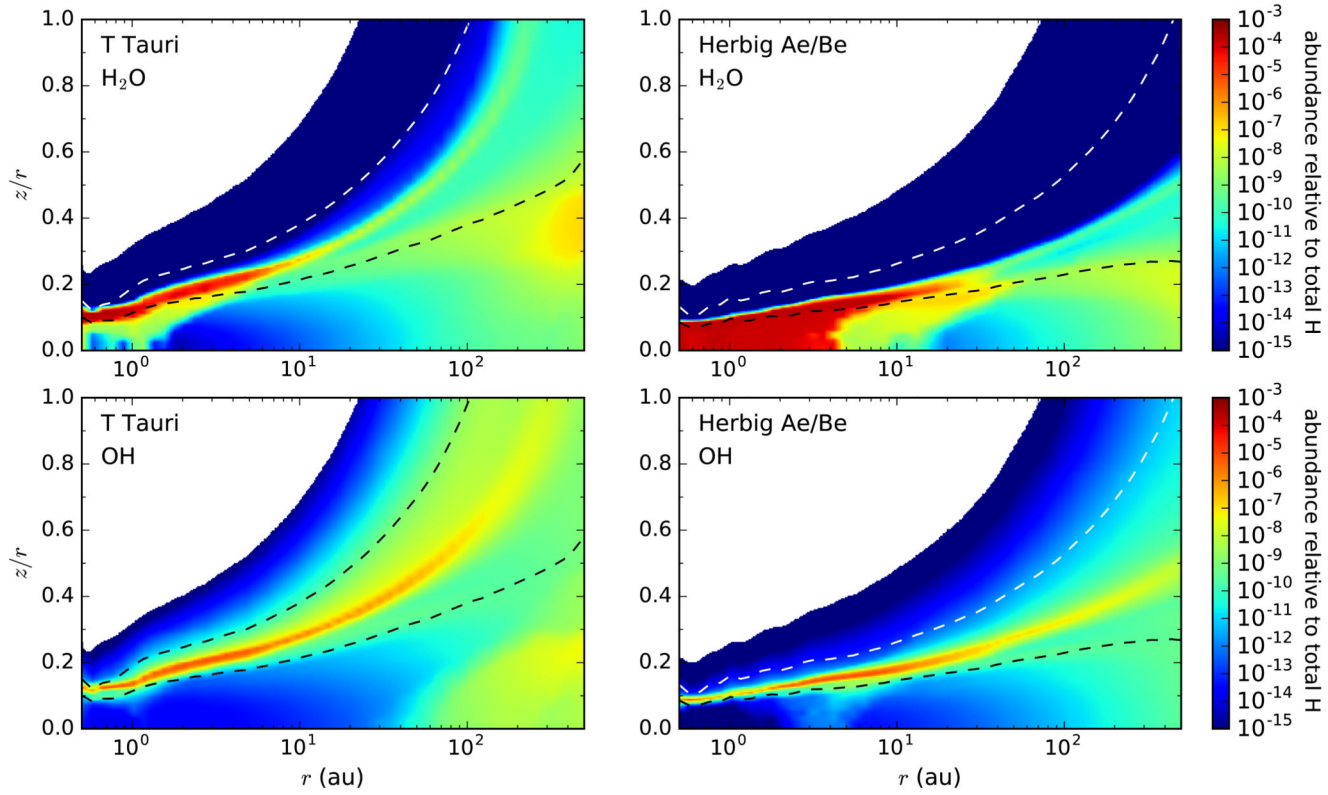

Fig. 4.

Calculated distributions of H_2O and OH as a function of radius r and height over radius z/r for the T Tauri (left) and Herbig Ae/Be (right) disks. The dashed lines indicate the location where A_V in the outward vertical direction takes values of 0.01 and 1.

Europe PMC Funders Author Manuscripts

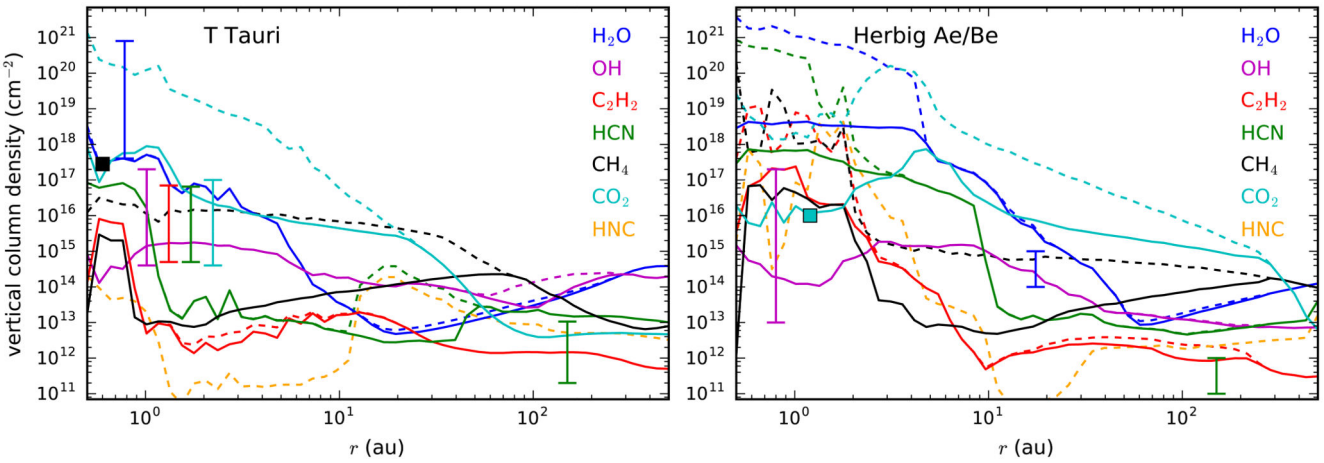

Fig. 5.

Calculated vertical column densities down to the A_V=10 surface (solid lines) and down to the midplane (dashed lines) of H_2O, OH, and simple organics as a function of radius r for the T Tauri (left panel) and Herbig Ae/Be (right panel) disks. For HNC, only the total column density down to the midplane is shown. Column densities derived from observations are indicated by vertical lines (when there are ranges of values) or by squares (when only one value is available), with their radial locations corresponding to the approximate region probed by observations (see Table 3).

Europe PMC Funders Author Manuscripts

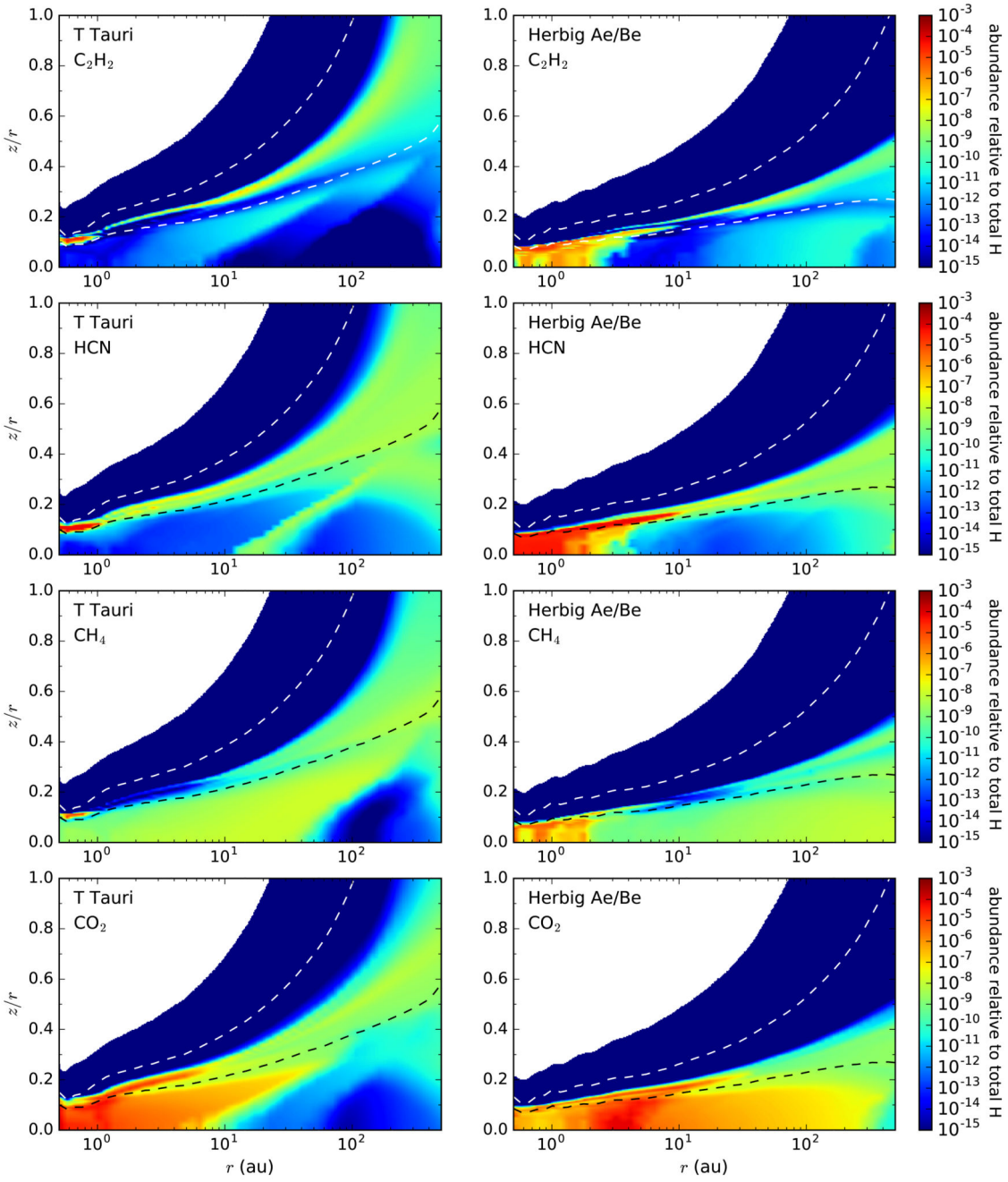

Fig. 6.
Same as Fig. 4 but for C_2H_2, HCN, CH_4, and CO_2.

Europe PMC Funders Author Manuscripts

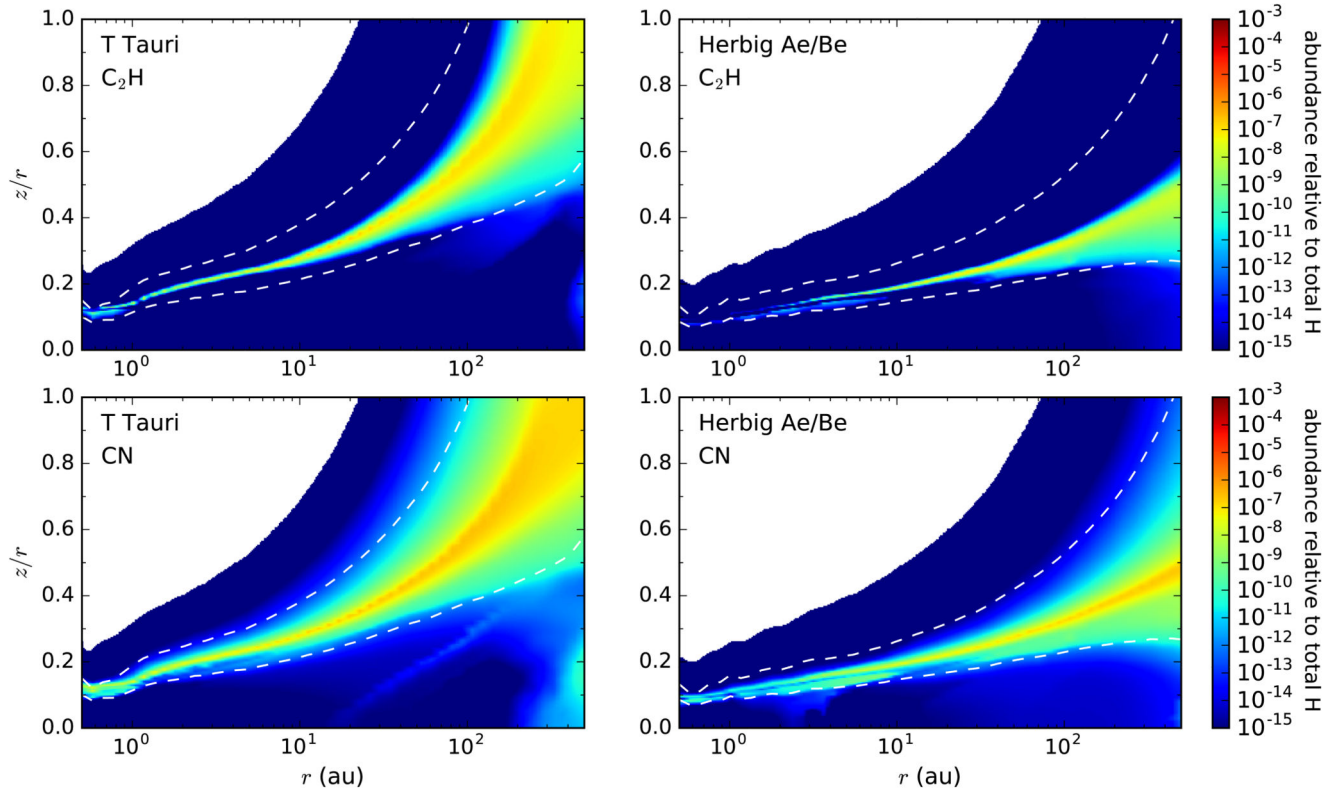

Fig. 7.
Same as Fig. 4 but for C_2H and CN.

Europe PMC Funders Author Manuscripts

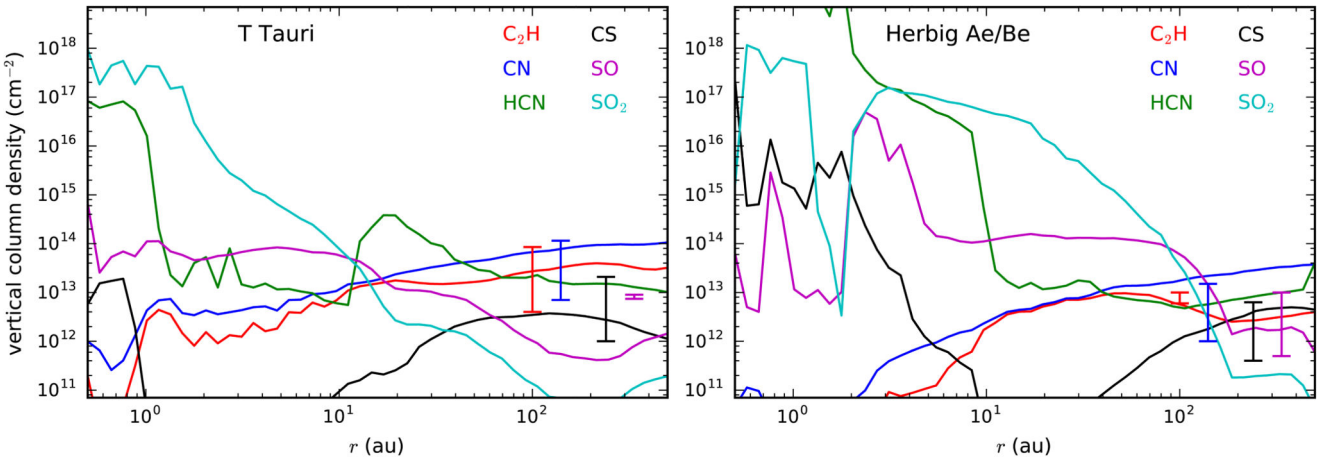

Fig. 8.

Calculated vertical column densities (down to the midplane) of the radicals C_2H and CN and some sulfur-bearing molecules as a function of radius *r* for the T Tauri (left panel) and Herbig Ae/Be (right panel) disks. HCN is also shown to allow for the visualization of the CN/HCN ratio. The ranges of column densities derived from observations are indicated by the vertical lines plotted in the outer disk (see Table 3).

Europe PMC Funders Author Manuscripts

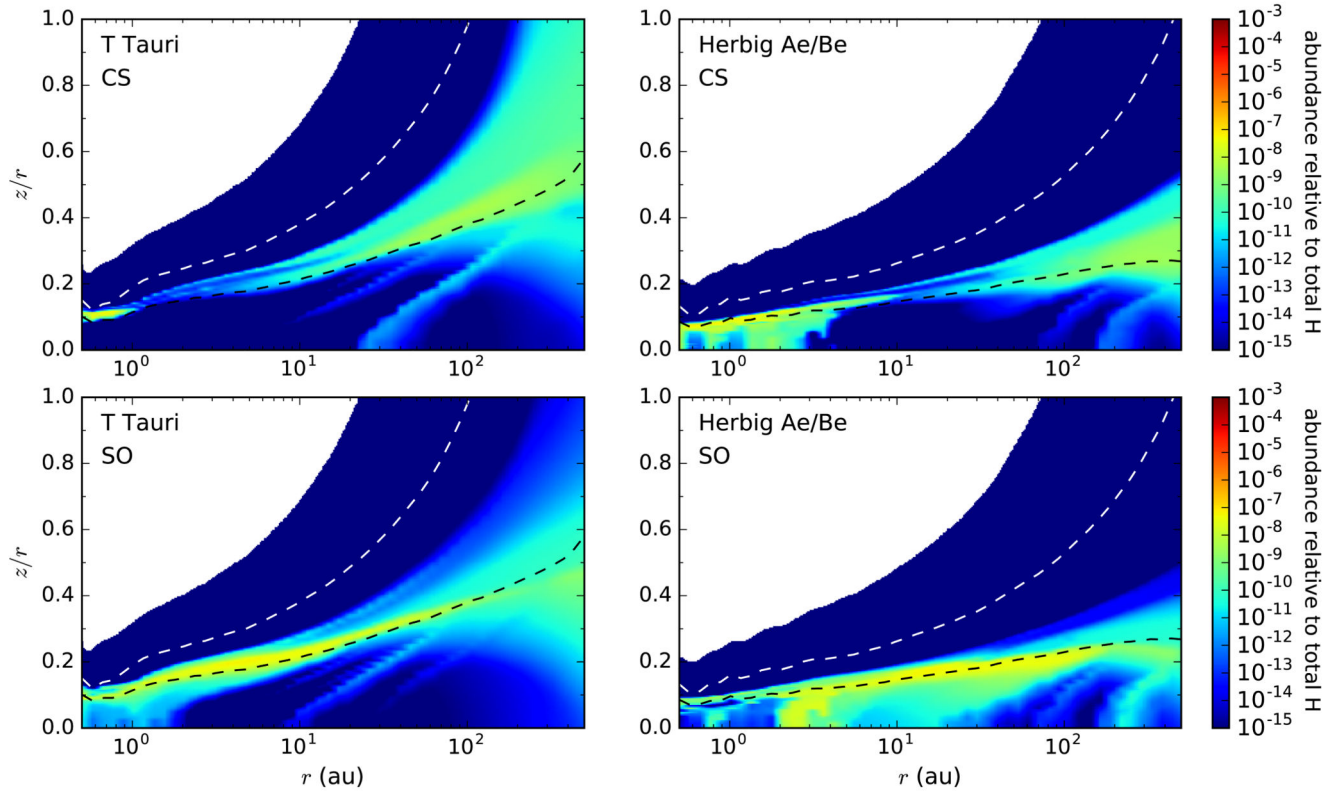

Fig. 9.
Same as Fig. 4 but for CS and SO.

Europe PMC Funders Author Manuscripts

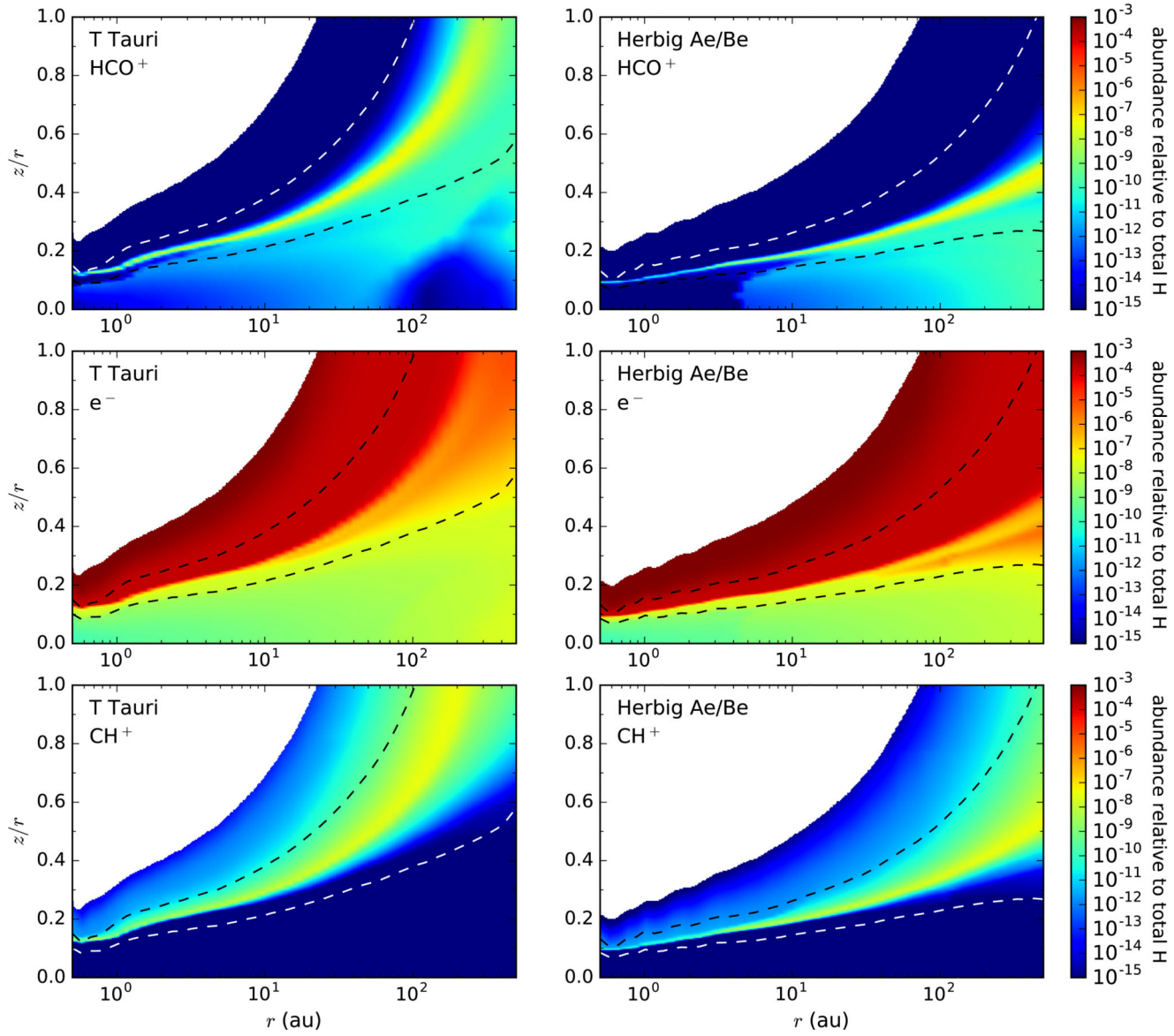

Fig. 10.
Same as Fig. 4 but for HCO^+, electrons, and CH^+.

Europe PMC Funders Author Manuscripts

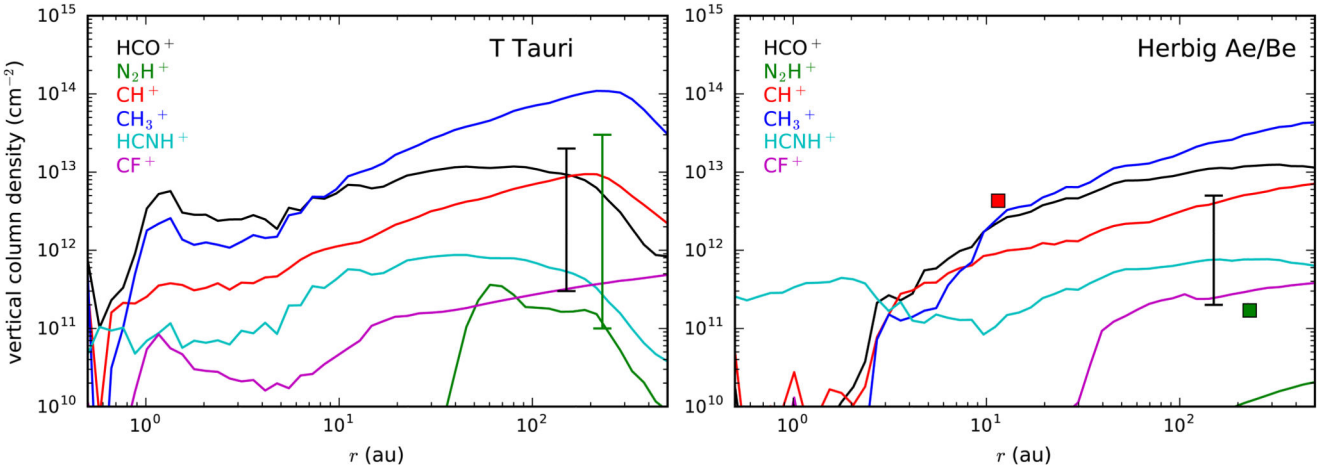

Fig. 11.

Calculated vertical column densities (down to the midplane) of selected molecular ions as a function of radius *r* for the T Tauri (left panel) and Herbig Ae/Be (right panel) disks. Column densities derived from observations are indicated by vertical lines or squares, with their radial locations corresponding to the approximate region probed by observations (see Table 3).

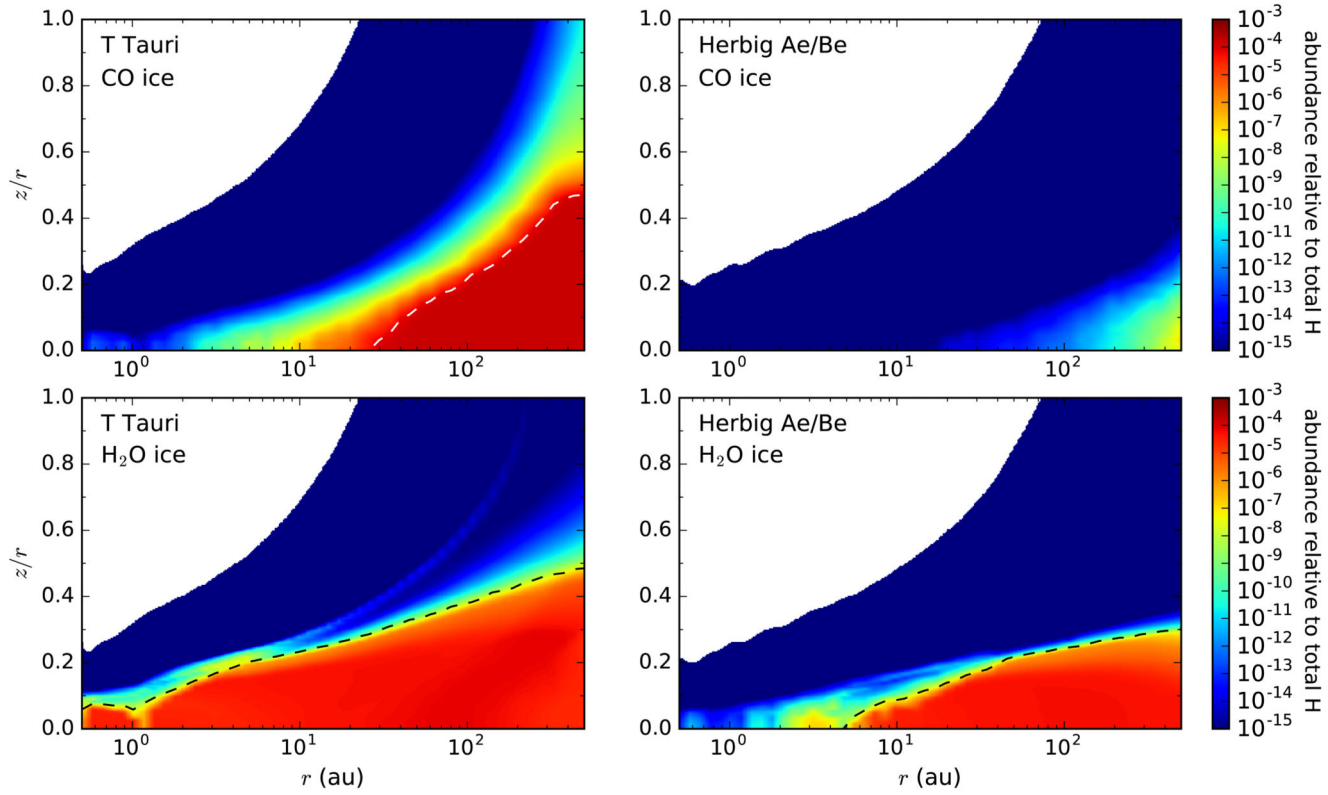

Fig. 12.

Calculated distributions of CO and H_2O ices as a function of radius *r* and height over radius *z/r* for the T Tauri (left) and Herbig Ae/Be (right) disks. The dashed line in each panel indicates the location of the corresponding snowline.

Europe PMC Funders Author Manuscripts

Europe PMC Funders Author Manuscripts

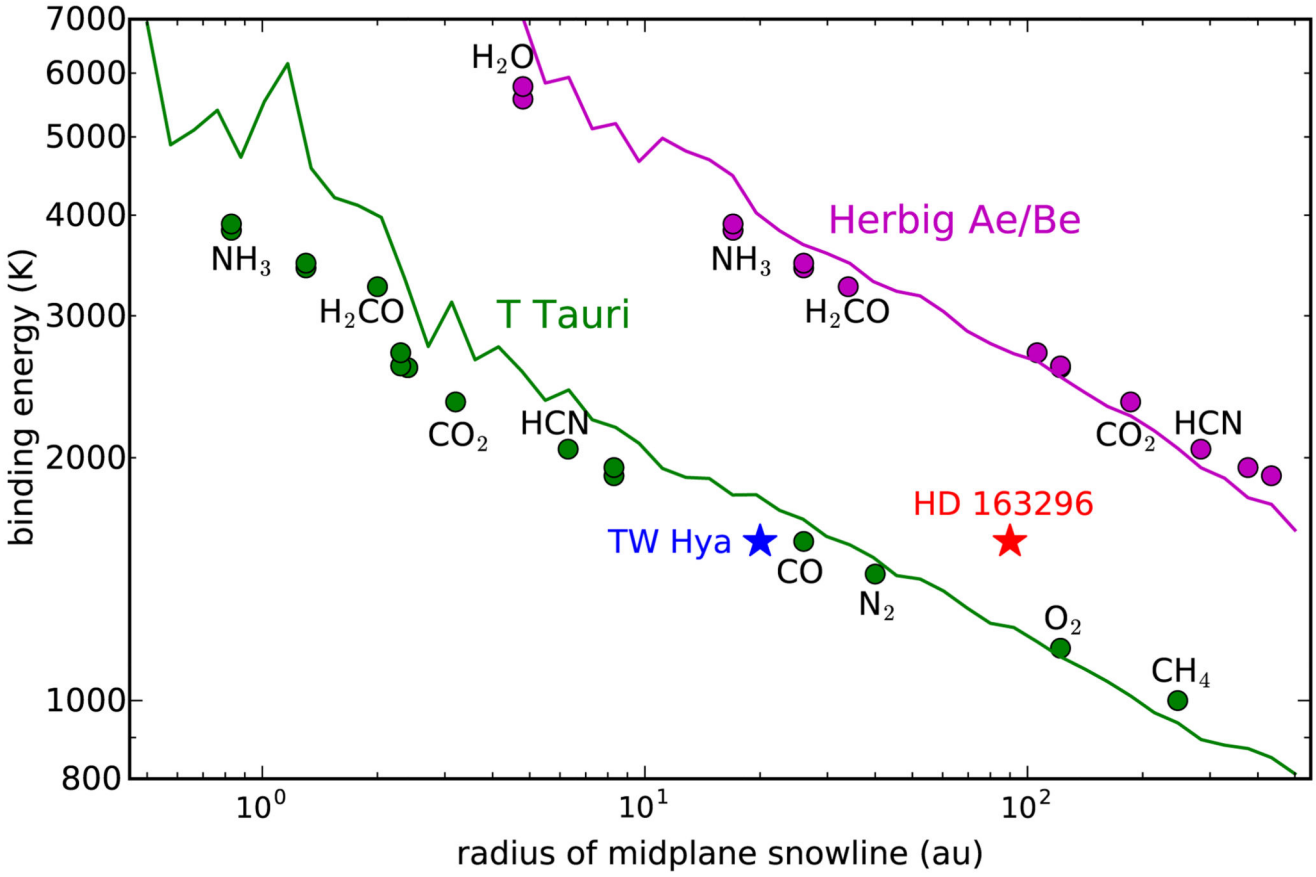

Fig. 13.

Midplane snowline of various ices (along *x*-axis) as a function of the binding energy (along *y*-axis) in the T Tauri (green circles) and Herbig Ae/Be (magenta circles) disks. Observational CO snowlines in TW Hya (Schwarz et al. 2016; Zhang et al. 2017) and HD 163296 (Qi et al. 2015) are also shown. We also plot the dust temperature in the midplane (scaled up by a factor of 45) as a function of radius in the T Tauri (green solid line) and Herbig Ae/Be (magenta solid line) disk models.

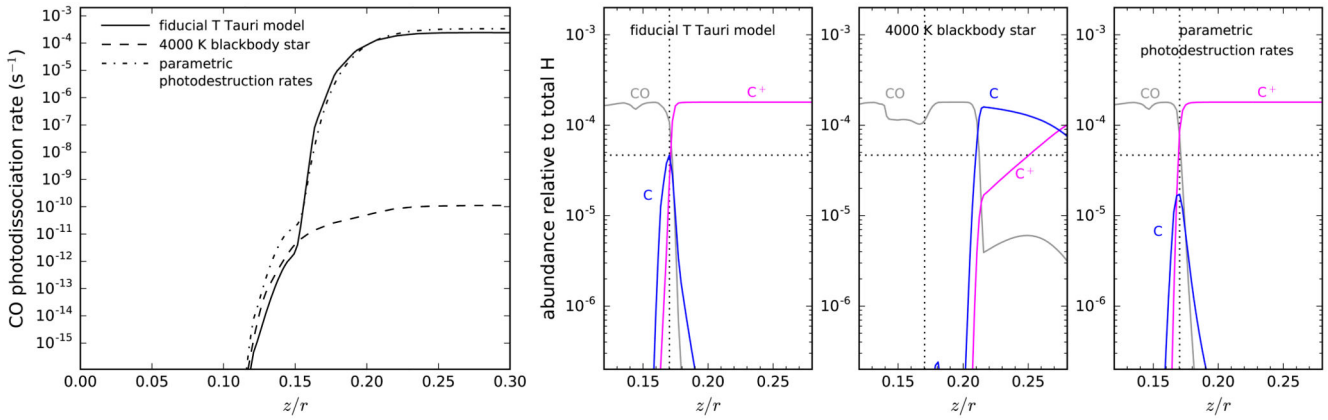

Fig. 14.

Vertical structure of the CO photodissociation rate (left panel) and the CO/C/C$^+$ interface (right panels) at a radius of 1 au from the star for the T Tauri disk. We show results from our fiducial model, a model in which a 4000 K blackbody stellar spectrum is considered, and a model in which all photodestruction rates are computed using parametric expressions (see text). The dotted lines in the three right panels indicate what is the peak abundance of atomic carbon and at which height it is reached in the fiducial model. The small drop in the abundance of CO seen around $z/r \sim 0.15$, which is more marked in the 4000 K blackbody star model, is due to a maximum in the abundance of water.

Europe PMC Funders Author Manuscripts

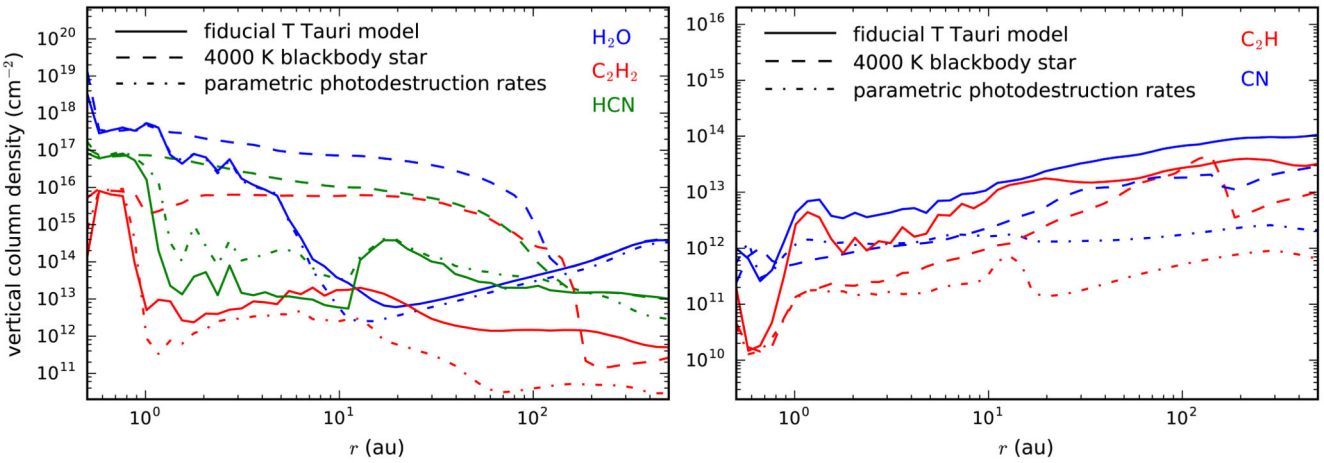

Fig. 15.

Calculated vertical column densities down to the midplane of H_2O, C_2H_2, and HCN (left panel) and the radicals C_2H and CN (right panel) as a function of radius *r* for the T Tauri disk. We show results from our fiducial model, a model in which a 4000 K blackbody stellar spectrum is considered, and a model in which all photodestruction rates are computed using parametric expressions (see text).

Europe PMC Funders Author Manuscripts

Europe PMC Funders Author Manuscripts

Table 1

Model parameters.

Parameter	Value / Source
Disk	
Disk mass (M_{disk})	0.01 $M_\odot$
Inner disk radius (R_{in})	0.5 au
Outer disk radius (R_{out})	500 au
Radial surface density power index (ϵ)	1.0 †
Gas-to-dust mass ratio (ρ_g/ρ_d)	100
Dust composition	70 % silicate 30 % graphite
Minimum dust grain radius (a_{min})	0.001 μm
Maximum dust grain radius (a_{max})	1 μm
Dust size distribution power index (β)	3.5
Interstellar radiation field	Draine (1978)
Cosmic-ray ionization rate of H_2(ζ)	5×10^{-17} s^{-1}
T Tauri star	
Stellar mass (M_*)	0.5 $M_\odot$
Stellar radius (R_*)	2 $R_\odot$
Stellar effective temperature (T_*)	4000 K
Herbig Ae/Be star	
Stellar mass (M_*)	2.5 $M_\odot$
Stellar radius (R_*)	2.5 $R_\odot$
Stellar effective temperature (T_*)	10,000 K

† $\epsilon = -12$ at $r < R_{in}$.

Table 2

Ice species, binding energies, and photodesorption yields.

Species	E_D (K)	Ref.	Y (molecule photon^{-1})	Ref.
CH_4	1000	*(1)* ◊	10^{-3}	*(11)*
C_2H_2	2587	*(2)* ‡	10^{-3}	*(11)*
C_2H_4	3487	*(2)* ‡	10^{-3}	*(11)*
C_2H_6	4387	*(2)* ‡	10^{-3}	*(11)*
H_2O	5773	*(3)* ◊	$(1.3 + 0.032\ T_d) \times 10^{-3}$	*(12)* *
O_2	1161	*(4)* † ♮	$(2.8^a, 2.3^b, 2.4^c) \times 10^{-3}$	*(13)* §
CO	1575	*(5)* † ♮	$(9.5^a, 4.8^b, 10.3^c) \times 10^{-3}$	*(14)* §
CO_2	2346	*(4)* † ♮	$(8.2^a, 2.0^b, 0.98^c) \times 10^{-4}$	*(15)* § *
H_2CO	3260	*(6)* †	10^{-3}	*(11)*
CH_3OH	4990	*(7)* ◊	$(1.5^a, 1.1^b, 1.3^c) \times 10^{-4}$	*(16)* § *
HCOOH	5570	*(2)* ‡	10^{-3}	*(11)*
NH_3	3830	*(1)* ◊	10^{-3}	*(11)*
N_2	1435	*(5)* † ♮	$(2.0^a, 1.6^b, 0.89^c) \times 10^{-3}$	*(13)* §
HCN	2050	*(2)* ‡	10^{-3}	*(11)*
H_2S	1945	*(8)* ♯	10^{-3}	*(11)*
CS	1900	*(2)* ‡	10^{-3}	*(11)*
H_2CS	2700	*(2)* ‡	10^{-3}	*(11)*
SO	2600	*(2)* ‡	10^{-3}	*(11)*
SO_2	3900	*(9)* †	10^{-3}	*(11)*
OCS	3440	*(10)* ◊	10^{-3}	*(11)*

Notes.– ◊ pure ice; † amorphous water ice substrate (♮ submonolayer regime); ♯ solid SO_2 substrate; ‡ estimated for water ice substrate; § wavelength-dependent photodesorption yield is convolved over the 7-13.6 eV range with the interstellar^a, T Tauri^b, and Herbig Ae/Be^c FUV radiation fields described in section 2.1.1; * yields of direct photodesorption and fragmentation have been measured.

References.– (1) Luna et al. (2014); (2) Garrod & Herbst (2006); (3) Fraser et al. (2001); (4) Noble et al. (2012a); (5) Fayolle et al. (2016); (6) Noble et al. (2012b); (7) Doronin et al. (2015); (8) Sandford & Allamandola (1993); (9) Schriver-Mazzuoli et al. (2003), assuming that E_D is directly proportional to the desorption temperature (see, e.g., Martín-Doménech et al. 2014); (10) Burke & Brown (2010); (11) assumed; (12) pure H_2O ice (> 8 ML) in the 18-100 K range; the fraction of H_2O molecules photodesorbed is $(0.42 + 0.002\ T_d)$, the remaining results in fragmentation into OH + H (Öberg et al. 2009); (13) pure O_2 (30 ML) and $^{15}N_2$ (60 ML) ices at 15 K (Fayolle et al. 2013); (14) pure CO ice (10 ML) at 18 K (Fayolle et al. 2011); (15) pure $^{13}CO_2$ (10 ML) ice at 10 K; the fraction of CO_2 molecules desorbed is 0.37, 0.42, and 0.22 under the interstellar, T Tauri, and Herbig Ae/Be FUV fields, respectively, the remaining results in fragmentation into CO + O (Fillion et al. 2014); (16) pure CH_3OH (20 ML) ice at 10 K; the fraction of CH_3OH molecules desorbed is 0.08, while the fragmentation channels CH_3 + OH, H_2CO + H_2, CO + H_2 + H_2 occur with fractions of 0.05, 0.07, and 0.80, almost independently of the radiation field (Bertin et al. 2016; see also Cruz-Diaz et al. 2016).

Table 3

Summary of molecules (other than H_2 and CO) observed in disks and abundances derived.

Species	Spectral signature, region probed	Detection rate, abundance, and references			
		T Tauri		Herbig Ae/Be	
H_2O	IR emission, inner atmosphere	many disks $(0.4 - 800) \times 10^{18}$ cm^{-2}	*(1,2,3,4,5,6,7,8,9,10,11)* *(6,7)*	one disk: HD 163296 $10^{14} - 10^{15}$ cm^{-2}	*(4,7,11,12,13,14,15)* *(14)*
	sub-mm emission, outer disk	two disks: TW Hya, DGTau ~ 10^{-7} relative to H_2	*(16,17,18)* *(16)*	one disk: HD 100546	*(18,19)*
OH	IR emission, inner atmosphere	many disks $(0.4 - 200) \times 10^{15}$ cm^{-2}	*(2,3,4,6,7,8,11,15,20)* *(6,7)*	a dozen of disks $(0.01 - 200)$ x 10^{15} cm^{-2}	*(4,7,11,12,21)* *(12,15,21)*
C_2H_2	IR emission/ absorption, inner disk	many disks $(0.5 - 70) \times 10^{15}$ cm^{-2}	*(2,6,7,8,22,23,24)* *(6,7,22,23,24)*	none	
HCN	IR emission/ absorption, inner disk	many disks $(0.5 - 65) \times 10^{15}$ cm^{-2}	*(2,6,7,8,22,23,24)* *(6,7,22,23,24)*	none	
	mm emission, outer disk	many disks $(0.2 - 10.6) \times 10^{12}$ cm^{-2}	*(27,28,29,30,31,32,33,35)* *(28,31,32,33)*	many disks $(0.1 - 1) \times 10^{12}$ cm^{-2}	*(28,29,30,31,32,33,34)* *(31,33,34)*
HNC	mm emission, outer disk	two disks: DM Tau, TW Hya HNC/HCN = 0.3-0.4	*(27,36)* *(27)*	one disk: HD 163296 HNC/HCN = 0.1 − 0.2	*(36)* *(36)a*
CH_4	IR absorption, inner disk	one disk: GV Tau 2.8×10^{17} cm^{-2}	*(25)* *(25)*	none	
CO_2	IR emission/ absorption, inner disk	many disks $(0.04 - 10) \times 10^{16}$cm^{-2}	*(6,7,22,24,26)* *(7,22,24,26)*	one disk: HD 101412 10^{16} cm^{-2}	*(7)* *(7)*
C_2H	mm emission, outer disk	many disks $(0.4 - 8.5) \times 10^{13}$cm^{-2}	*(27,32,33,37,38)* *(33,37)b*	two disks: AB Aur, MWC 480 $(0.6 - 1) \times 10^{13}$ cm^{-2}	*(33,34,37,39,40)* *(33)*
CN	mm emission, outer disk	many disks $(0.7 - 11.5) \times 10^{13}$ cm^{-2}	*(27,28,29,30,31,32,33)* *(28,31,32,33)*	a handful of disks $(0.1 - 1.5) \times 10^{13}$ cm^{-2}	*(28,29,30,31,33,34)* *(28,31,33,34)*
H_2CO	mm emission, outer disk	a dozen of disks $(0.9 - 4.4) \times 10^{12}$ cm^{-2}	*(27,28,29,30,33,41,43,44)* *(33)c*	a handful of disks $(1.6 - 3.3) \times 10^{12}$ cm^{-2}	*(30,33,34,42,45,46)* *(33)d*
CH_3OH	mm emission (ALMA), outer disk	one disk: TW Hya; $(3 - 6) \times 10^{12}$ cm^{-2}	*(47)*	none	
HC_3N	mm emission, outer disk	two disks: GO Tau, LkCa 15; ~ 10^{12} cm^{-2}	*(48)*	one disk: MWC 480; ~ 10^{12} cm^{-2}	*(48,49)*
CH_3CN	mm emission (ALMA), outer disk	none		one disk: MWC 480; ~ 10^{13} cm^{-2}	*(49)*
c-C_3H_2	mm emission (ALMA), outer disk	one disk: TW Hya	*(38)*	one disk: HD 163296; $10^{12} - 10^{13}$ cm^{-2}	*(50)*
NH_3	sub-mm emission, outer disk	one disk: TW Hya	*(51)* *(51)*	none	

Species	Spectral signature, region probed	Detection rate, abundance, and references			
		T Tauri		Herbig Ae/Be	
		$(0.2 - 17) \times 10^{-11}$ relative to H_2			
CS	mm emission, outer disk	a dozen of disks $(1 - 20.9) \times 10^{12}$ cm^{-2}	*(27,32,33,52)* *(32,33,52)*	two disks: AB Aur, MWC 480 $(0.4 - 6.3) \times 10^{12}$cm^{-2}	*(33,34,40)* *(33,34)*
SO	mm emission, outer disk	two disks: CI Tau, GM Aur $(7.4 - 9) \times 10^{12}$ cm^{-2}	*(33)* *(33)*	one disk: AB Aur $(0.5 - 10) \times 10^{12}$ cm^{-2}	*(33,34,40,42)* *(33,34,42)*
HCO^+	mm emission, outer disk	many disks $(0.3 - 20) \times 10^{12}$ cm^{-2}	*(28,29,30,33,35,53,54,55)* *(28,33,53,54,55)*	many disks $(0.2 - 5) \times 10^{12}$ cm^{-2}	*(28,29,30,33,34,54,56)* *(28,33,34,54)e*
N_2H^+	mm emission, outer disk	a handful of disks $(0.1 - 30) \times 10^{12}$ cm^{-2}	*(29,30,44,53,54,57)* *(53,54)f*	one disk: HD 163296 1.7×10^{11} cm^{-2}	*(45)* *(45)*
CH^+	sub-mm emission, mid disk	none		two disks: HD 100546, HD 97048 4.3×10^{12} cm^{-2}	*(15,58)* *(58)g*

References: (1) Carr et al. (2004); (2) Carr & Najita (2008); (3) Salyk et al. (2008); (4) Pontoppidan et al. (2010a); (5) Pontoppidan et al. (2010b); (6) Carr & Najita (2011); (7) Salyk et al. (2011); (8) Mandell et al. (2012); (9) Riviere-Marichalar et al. (2012); (10) Sargent et al. (2014); (11) Banzatti et al. (2017); (12) Fedele et al. (2011); (13) Meeus et al. (2012); (14) Fedele et al. (2012); (15) Fedele et al. (2013); (16) Hogerheijde et al. (2011); (17) Podio et al. (2013); (18) Du et al. (2017); (19) van Dishoeck et al. (2014); (20) Carr & Najita (2014); (21) Mandell et al. (2008); (22) Lahuis et al. (2006); (23) Gibb et al. (2007); (24) Bast et al. (2013); (25) Gibb & Horne (2013); (26) Kruger et al. (2011); (27) Dutrey et al. (1997); (28) Thi et al. (2004); (29) Öberg et al. (2010); (30) Öberg et al. (2011); (31) Chapillon et al. (2012a); (32) Kastner et al. (2014); (33) Guilloteau et al. (2016); (34) Fuente et al. (2010); (35) Fuente et al. (2012); (36) Graninger et al. (2015); (37) Henning et al. (2010); (38) Bergin et al. (2016); (39) Schreyer et al. (2008); (40) Pacheco-Vázquez et al. (2015); (41) Aikawa et al. (2003); (42) Pacheco-Vázquez et al. (2016); (43) Loomis et al. (2015); (44) Öberg et al. (2017); (45) Qi et al. (2013a); (46) Carney et al. (2017); (47) Walsh et al. (2016); (48) Chapillon et al. (2012b); (49) Öberg et al. (2015); (50) Qi et al. (2013b); (51) Salinas et al. (2016); (52) Dutrey et al. (2011); (53) Qi et al. (2003); (54) Dutrey et al. (2007); (55) Teague et al. (2015); (56) Mathews et al. (2013); (57) Qi et al. (2013c); (58) Thi et al. (2011).

Notes:

[a] Values are line intensity ratios rather than abundance ratios.

[b] Out of this range, Kastner et al. (2014) derive $N(C_2H) = 5.1 \times 10^{15}$ cm^{-2} in TW Hya.

[c] Out of this range, Aikawa et al. (2003) derive $N(H_2CO) = (7.2 - 19) \times 10^{12}$ cm^{-2} in LkCa 15.

[d] Carney et al. (2017) derive a H_2CO abundance of $(2 - 5) \times 10^{-12}$ relative to H_2 in HD 163296.

[e] Out of this range, Mathews et al. (2013) derive $N(HCO^+) = 1.5 \times 10^{14}$ cm^{-2} in HD 163296.

[f] Out of this range, Qi et al. (2013c) derive $N(N_2H+) = 10^{14} - 10^{15}$ cm^{-2} in TW Hya.

[g] In the same object, HD 100546, Fedele et al. (2013) derive $N(CH^+) = 10^{16} - 10^{17}$ cm^{-2} for an emitting area inner to 50-70 au.